Coherent Optical Focal Plane Array Receiver for PPM Signals: Investigation and Applications

Michela Muñoz Fernández*[ab]

[a]California Institute of Technology, 1200 E. California Blvd., Pasadena, CA 91125
[b]Jet Propulsion Laboratory, California Institute of Technology, 4800 Oak Grove Dr., Pasadena, CA 91109

ABSTRACT

The performance of a coherent optical focal plane array receiver for PPM signals under atmospheric turbulence is investigated and applications of this system are addressed. The experimental demonstration of this project has already been explained in previous publications [1]. This article shows a more exhaustive analysis of the expressions needed to obtain the Bit Error Rate (BER) for the real system under study in the laboratory. Selected experimental results of this system are described and compared with theoretical BER expressions, and array combining gains are presented. Receiver sensitivity in terms of photons per bit (PPB) is examined; BER results are shown as a function of signal to noise ratios, (SNR), as well as a function of photons per symbol, and photons per bit.

Keywords: focal plane array, coherent optical communications, shot noise limited performance.

1. Introduction

A heterodyne detection system was selected for this investigation for deep space optical communications with noncoherent demodulation since this choice should improve receiver sensitivity by 3 dB compared to that of a direct detection system [2]. The choice of noncoherent demodulation is motivated to a high degree by the physics of the problem. A difficulty that arises with PPM modulation is that no signal is present except in the signal slots. This makes it infeasible, in some but not all cases, to use a phase-locked loop (PLL) to track a signal carrier for two reasons. The loop can lose lock when the PPM pulse is over, and the duration of a PPM pulse may not give the loop adequate time to reacquire lock. Hence, the most common technique for maintaining phase synchronization in communications systems often will not apply.

At this point, it is useful to examine the meaning of the term "coherent." The optical receiver that is the subject of this work is optically coherent. Instead of performing photon counting, it mixes the incoming optical signal with a locally generated local oscillator laser to produce an intermediate frequency (IF) communications signal that can be demodulated and processed using traditional methods. Hence, the term "optically coherent" will be used in reference to systems that mix incoming laser signals with a local oscillator laser and demodulate the resulting IF signal. This term differs from the term "coherent" in the communications context. In communications systems, the term "coherent" is used in reference to those systems that are able to track the phase of the incoming signal. Since this is not always a feasible task, a non-coherent envelope detection communications receiver was chosen.

The research described in this publication was carried out at the Jet Propulsion Laboratory, California Institute of Technology, under a contract with the National Aeronautics and Space Administration.

*Email: Michela.Munoz.Fernandez@jpl.nasa.gov, phone 1 818 354-5046; fax 1 818 393 6871; jpl.nasa.gov

The choice of a focal plane array based receiver [9] instead of a single detector based receiver was driven by the presence of atmospheric turbulence. Even in clear weather there are random, time-varying patterns in the index of refraction of the air in the Earth's atmosphere. When a laser signal from a distance spacecraft (assumed to be a plane wave due to the tremendous distances involved in deep space communications) passes through the atmosphere, the differences in refractive index will distort the planar phase front of the incoming signal wave. This causes the wavefront that reaches the receiving telescope aperture to suffer from significant phase distortions that will cause the received signal pattern in the receiver focal plane to be spread out and be significantly distorted. A single small detection element designed to capture the Airy pattern resulting from a perfect plane wave reaching the aperture will be too small to catch most of the signal, resulting in severe signal losses. One could attempt to compensate for the spreading of the signal in the detector focal plane by using a single very large receiving element in the focal plane. However, the field in the focal plane is a complex field with both magnitude and phase. A single large detector element will effectively perform a simple addition of the focal plane field over its surface, and this could easily result in *destructive* signal cancellation, again resulting in severe signal losses. The key to capturing the scattered, phase and amplitude distorted signal field in the focal plane is to have an array of small elements. As signal components of varying amplitude and phase hit the array, the outputs of the receiving elements are coherently added together in order to reconstruct the original signal, avoiding both the self-cancellation that often occurs with large detection elements and the waste of useful signal energy in the focal plane that results from having a single small detection element incapable of capturing the entire signal field.

The selection of the size and geometry of a coherent optical focal plane array will be driven by a series of key factors [9]:

1. The wavelength λ of the signal laser.
2. The diameter D of the telescope aperture.
3. The focal length f of the telescope.
4. The Fried parameter r_0 that characterizes turbulence. This parameter is described in greater detail below.

It is assumed that the incoming signal wavefront is of unit amplitude and also that it suffers from phase distortions induced by atmospheric turbulence following Kolmogorov's model [3]. This turbulence is characterized by a coherence length r_0. It is generally assumed that the phase does not experience RMS fluctuations of more than one radian over a distance r_0 in the incoming wavefront. A low value of r_0 implies an atmospheric phase screen with great phase changes over a short scale. A high value of r_0 implies an atmospheric phase screen with high spatial correlation whose phase varies slowly as a function of distance.

It is well known that the approximate diameter of the Airy pattern in the focal plane of a telescope is $\frac{\lambda f}{D}$ (based on the Fourier transform relationship between the aperture plane and focal plane fields [4] if the wavefront reaching the telescope aperture is an ideal plane wave. It is also known that the average size of the spread and distorted focal plane field in the presence of Kolmogorov turbulence is approximately $\frac{\lambda f}{r_0}$. Hence, the presence of atmospheric turbulence will increase the diameter of the signal field in the focal plane by a factor of approximately $\frac{D}{r_0}$. For example, a one-meter diameter telescope operating with $r_0 = 0.1\ \mathrm{m}$ will see a tenfold increase in its focal plane spot diameter. The need for a focal plane array to capture all of this energy for coherent recombining is now clear.

The need for *adaptive* coherent combining algorithms is a direct result of the fact that the random refractive index fluctuations in the atmosphere that spread and distort the focal plane field are rapidly time-varying fluctuations that must be tracked by an adaptive algorithm.

The detector elements of the coherent FPA can be thought of as sampling units that capture real-time samples of the complex focal plane field. Such samples can be used to reconstruct the focal plane field as long as the Nyquist criterion for spatial sampling is met.

Let the complex field in the focal plane of the detector by denoted $U_f(\rho,\phi)$, where the coordinate pair (ρ,ϕ) is the polar coordinate pair in the focal plane. Likewise, let the complex field in the aperture plane of the receiver be denoted by $U_a(r,\theta)$. The aperture is assumed to be circular with radius *R*. Then the relationship between the aperture plane and focal plane fields is given by [4]:

$$U_f(\rho,\phi) = \frac{\exp\left(j\frac{k}{2f}\rho^2\right)}{j\lambda f}\int_0^R\int_{-\pi}^{\pi} U_a(r,\theta)\exp\left(-j\frac{2\pi}{\lambda f}r\rho\cos(\theta-\phi)\right)rd\theta dr \qquad (1)$$

where we define:

1. λ: The wavelength of the light
2. *k*: The wave number, $\frac{2\pi}{\lambda}$
3. *f*: The effective focal length of the receiver telescope
4. *R*: The radius of the receiving telescope aperture, which is *D*/2

Equation (1) is a Fourier transform relationship [4] and is fully invertible. Given that the finite aperture radius *R* imposes a spatial frequency limit on the complex field in the focal plane, there exists a spatial sampling interval $R_s = \frac{\lambda f}{2R} = \frac{\lambda f}{D}$ such that rectangular point sampling with this spacing in the focal plane will permit perfect reconstruction of the original signal [4]. If the FPA detector elements are taken as point sampling functions [5] and if the FPA detector grid captures almost all of the energy in the focal plane field, then a detector grid spacing interval of R_s or less will permit the focal plane field $U_f(\rho,\phi)$ to be reconstructed using sinc-function interpolation [4]. An inverse Fourier transform operation could then be used to reconstruct the aperture plane field $U_a(r,\theta)$.

Reconstruction of the aperture plane field has many benefits. In particular, the aperture plane field yields useful real-time information on the phase perturbations introduced by the atmosphere while the optical communications channel is running. Such data can be of value to the atmospheric science community and is also of engineering value when deep space optical communications links are designed.

2. Probability of bit error for non-coherent (heterodyne) optical receiver with random phase channels for pulse position modulated (PPM) signals

2.1. Case I: Probability of bit error for the single channel

The expression for the probability of bit error for the single channel non-coherent receiver may be expressed [6]:

$$P_b(E) = \frac{M/2}{M-1} \sum_{m=1}^{M-1} (-1)^{m+1} \frac{1}{m+1} {}_{M-1}C_m \exp\left\{ -\frac{m}{m+1} \left(\frac{E_s}{N_0} \right) \right\} \tag{2}$$

with $E_s / N_0 = SNR$ of the channel under study, M is the PPM order, and where ${}_{M-1}C_m = \frac{(M-1)!}{m!(M-1)!}$.

2.2. Case II: Probability of bit error with array combining

For the case of signals under AWGN, the probability of bit error is given by the same expression from Eq. (2), but instead of using the SNR of one channel, the right term to use is the addition of the SNR of the individual channels to be combined [7]. Expressing the SNR directly as a ratio instead of in decibels and letting $\left(\frac{E_S}{N_0} \right)_i$ denote the SNR of the ith channel, the total SNR is:

$$\left(\frac{E_S}{N_0} \right)_{total} = \sum_{i=1}^{N} \left(\frac{E_S}{N_0} \right)_i \tag{3}$$

for the case of N channels. Eq. (3) assumes that the noise is zero-mean Gaussian.

3. Probability of bit error for non-coherent (heterodyne) optical receiver with random phase channels for Pulse Position Modulated (PPM) signals in the presence of leakage in the noise slots

The derivations from previous sections assume a system model with zero mean noise variances for signal as well as noise slots. Theoretically that is the case to be expected, but the reality is that the equipment used for this thesis had some limitations and constraints, necessitating changes in the mathematical model. The PPM modulator is not ideal, and during the dead time it was "leaking" signal energy. This unwanted signal energy, referred to as "leakage," was mixed with the local oscillator laser, generating a heterodyned beatnote in the noise slots. This resulted in a non-zero signal mean in the noise slots, which in this section will be explained in more detail. Different channels presented different leakage characteristics that have been taken into account in the following signal model based on a non-central chi square distribution for the signal as well as the noise slots.

Previous sections analyzed the case of zero mean Gaussian random variables resulting in a central chi-square random variable with two degrees of freedom in the noise slots. If either or both of the Gaussian random variables has non-zero mean, then the result will be a non-central chi square random variable with two degrees of freedom. The central chi-square random variable is simply a special case of the non-central chi-square random variable [6].

First, consider the matched filter output in the signal slot. Since the signal consists of two Gaussian random variables with non-zero mean in the real and imaginary parts, the resulting pdf is a non-central chi-square pdf with two degrees of freedom. Let m_1 and m_2 be the means of the real and

imaginary parts of the complex Gaussian, and let them both have variance σ^2. Define the sum of the squares of the means:

$$s^2 = m_1^2 + m_2^2 \tag{4}$$

Then the pdf is given by:

$$f_{Y,sig}(y) = \frac{1}{2\sigma^2}\exp\left[-\frac{y+s^2}{2\sigma^2}\right] I_0\left(\frac{s\sqrt{y}}{\sigma^2}\right) \tag{5}$$

where $I_0(x)$ is the zeroth order modified Bessel function of the first kind.

If a leakage term is present in the noise slots, then the sum of squared means for those slots, s_L^2, will be non-zero. The resulting cdf will then be:

$$\begin{aligned} F_{Y,noise}(y) &= 1 - Q_1\left(\frac{s_L}{\sigma}, \frac{\sqrt{y}}{\sigma}\right) \\ &= 1 - \int_{\frac{\sqrt{y}}{\sigma}}^{\infty} x \exp\left(-\frac{x^2 + \left(\frac{s_L}{\sigma}\right)^2}{2}\right) I_0\left(\frac{s_L}{\sigma}x\right) dx \end{aligned} \tag{6}$$

where $Q_1(a,b)$ is the Marcum-Q function.

Plugging Eqs. (5) and (6) into the Eq. (7), [6] that is used to obtain the he probability of a correct decision

$$P(C) = \int_{-\infty}^{\infty} f_{Y,sig}(y)\left(F_{Y,noise}(y)\right)^{M-1} dy \text{ Eq.} \tag{7}$$

yields:

$$P(E) = 1 - \frac{1}{2\sigma^2}\int_0^{\infty} \exp\left[-\frac{y+s^2}{2\sigma^2}\right] I_0\left(\frac{s\sqrt{y}}{\sigma^2}\right)\left(1 - Q_1\left(\frac{s_L}{\sigma}, \frac{\sqrt{y}}{\sigma}\right)\right)^{M-1} dy \tag{8}$$

The integral in Eq. (8) presents the following difficulties:

1. It does not have a known closed form expression.
2. It is difficult to evaluate numerically for large M (i.e., $M = 256$).

One approach is to upper bound and lower bound the Marcum-Q function, and by using numerical bounds judiciously it is possible to obtain upper and lower bounds for the probability of symbol error given in Eq. (8). The bounds on the Marcum-Q function are given by [8];

$$\exp\left[-\frac{(b+a)^2}{2}\right] \le Q_1(a,b) \le \exp\left[-\frac{(b-a)^2}{2}\right] \tag{9}$$

The bounds in Eq. (9) play an important role in the analysis of the bit error probability performance of this system. Another possibility involves direct approximation of the integral in Eq. (8). The first stage is to expand the probability of correct decision as shown below:

$$
\begin{aligned}
P\left(\text{Correct Decision}\right) &= \int_0^\infty P\left(\text{Correct Decision}\middle| y\right) f_{Y,sig}\left(y\right) dy \\
&= \int_0^\infty \left(F_{Y,noise}\left(y\right)\right)^{M-1} f_{Y,sig}\left(y\right) dy \\
&= \int_0^\infty \left(F_{Y,noise}\left(y\right)\right)^{M-1} \left[\frac{1}{2\sigma^2}\exp\left(-\frac{y+s_{sig}^2}{2\sigma^2}\right) I_0\left(\frac{s}{\sigma^2}\sqrt{y}\right)\right] dy \\
&= \int_0^\infty \left(1-Q_1\left(\frac{s_{leak}}{\sigma},\frac{\sqrt{y}}{\sigma}\right)\right)^{M-1} \left[\frac{1}{2\sigma^2}\exp\left(-\frac{y+s_{sig}^2}{2\sigma^2}\right) I_0\left(\frac{s}{\sigma^2}\sqrt{y}\right)\right] dy_{sig}
\end{aligned}
\tag{10}
$$

Next, a binomial expansion is followed by an approximation step:

$$
\begin{aligned}
\left(1-Q_1\left(\frac{s_{leak}}{\sigma},\frac{\sqrt{y}}{\sigma}\right)\right)^{M-1} &= \sum_{m=0}^{M-1}\binom{M-1}{m}\left(-Q_1\left(\frac{s_{leak}}{\sigma},\frac{\sqrt{y}}{\sigma}\right)\right)^m \\
&\approx 1-\left(M-1\right)Q_1\left(\frac{s_{leak}}{\sigma},\frac{\sqrt{y}}{\sigma}\right)
\end{aligned}
\tag{11}
$$

The approximation from Eq. (11) is usable if the following condition is met:

$$
Q_1\left(\frac{s_{leak}}{\sigma},\frac{\sqrt{y_{sig}}}{\sigma}\right) \square \frac{1}{M-1} \tag{12}
$$

The approximation of Eq. (3.4.6) is used to simplify the integral:

$$
\begin{aligned}
&\int_0^\infty \left(1-Q_1\left(\frac{s_{leak}}{\sigma},\frac{\sqrt{y}}{\sigma}\right)\right)^{M-1} \left[\frac{1}{2\sigma^2}\exp\left(-\frac{y+s_{sig}^2}{2\sigma^2}\right) I_0\left(\frac{s}{\sigma^2}\sqrt{y}\right)\right] dy \\
&\approx \int_0^\infty \left[\frac{1}{2\sigma^2}\exp\left(-\frac{y+s_{sig}^2}{2\sigma^2}\right) I_0\left(\frac{s}{\sigma^2}\sqrt{y}\right)\right] dy - \\
&\left(M-1\right)\int_0^\infty Q_1\left(\frac{s_{leak}}{\sigma},\frac{\sqrt{y}}{\sigma}\right)\left[\frac{1}{2\sigma^2}\exp\left(-\frac{y+s_{sig}^2}{2\sigma^2}\right) I_0\left(\frac{s}{\sigma^2}\sqrt{y}\right)\right] dy \\
&= 1-\left(M-1\right)\int_0^\infty Q_1\left(\frac{s_{leak}}{\sigma},\frac{\sqrt{y}}{\sigma}\right)\left[\frac{1}{2\sigma^2}\exp\left(-\frac{y+s_{sig}^2}{2\sigma^2}\right) I_0\left(\frac{s}{\sigma^2}\sqrt{y}\right)\right] dy
\end{aligned}
\tag{13}
$$

The approximation used in Eq. (13) is very useful in that the integral on the last line has a closed form expression given by [8].

$$\int_0^\infty Q_1\left(\frac{s_{leak}}{\sigma},\frac{\sqrt{y}}{\sigma}\right)\left[\frac{1}{2\sigma^2}\exp\left(-\frac{y+s^2}{2\sigma^2}\right)I_0\left(\frac{s}{\sigma^2}\sqrt{y}\right)\right]dy$$
$$=Q_1\left(\frac{s_{leak}}{\sigma\sqrt{2}},\frac{s}{\sigma\sqrt{2}}\right)-\frac{1}{2}\exp\left(-\frac{s^2+s_{leak}^2}{4\sigma^2}\right)I_0\left(\frac{s\ s_{leak}}{2\sigma^2}\right) \tag{14}$$

The theoretical BER error rate can therefore be approximated using Eqs. (14) and (13) to obtain [9]:

$$\mathrm{SER}\left(s,s_{leak},\sigma\right)\approx\left(M-1\right)\left[Q_1\left(\frac{s_{leak}}{\sigma\sqrt{2}},\frac{s}{\sigma\sqrt{2}}\right)-\frac{1}{2}\exp\left(-\frac{s^2+s_{leak}^2}{4\sigma^2}\right)I_0\left(\frac{ss_{leak}}{2\sigma^2}\right)\right] \tag{15}$$

and

$$\mathrm{BER}\left(s,s_{leak},\sigma\right)=\frac{M/2}{M-1}\mathrm{SER}\left(s,s_{leak},\sigma\right)$$
$$\approx\frac{M}{2}\left[Q_1\left(\frac{s_{leak}}{\sigma\sqrt{2}},\frac{s}{\sigma\sqrt{2}}\right)-\frac{1}{2}\exp\left(-\frac{s^2+s_{leak}^2}{4\sigma^2}\right)I_0\left(\frac{s\ s_{leak}}{2\sigma^2}\right)\right] \tag{16}$$

Below a series of expressions specific to the case without leakage are given. If there is no leakage, then $s_L=0$ and the CDF $F_{Y,noise}\left(y\right)$ is then given by:

$$F_{Y,noise}\left(y\right)=1-Q_1\left(0,\frac{\sqrt{y}}{\sigma}\right) \tag{17}$$

This makes the upper and lower bounds in (9) equal to each other and therefore tight. It is now possible to write:

$$F_{Y,noise}\left(y\right)=1-\exp\left(-\frac{y}{2\sigma^2}\right) \tag{18}$$

The resulting expression for symbol error probability is:

$$1-\frac{1}{2\sigma^2}\int_0^\infty\exp\left[-\frac{y+s^2}{2\sigma^2}\right]I_0\left(\frac{s\sqrt{y}}{\sigma^2}\right)\left(1-\exp\left(-\frac{y}{2\sigma^2}\right)\right)^{M-1}dy \tag{19}$$

which is equivalent to the expression derived by [6] for *M*-ary orthogonal symbol error probabilities for non-coherent (from a communications perspective) receivers. Since:

$$\frac{E_S}{N_0}=\frac{s^2}{2\sigma^2} \tag{20}$$

is the SNR, it is possible to perform a change of variables in order to obtain symbol error probability as a function of SNR. The final answer in the no leakage case is [6]:

$$P\left(E\right)=\sum_{m=1}^{M-1}\left((-1)^{m+1}\frac{1}{m+1}\binom{M-1}{m}\exp\left(-\frac{m}{m+1}\left(\frac{E_S}{N_0}\right)\right)\right) \tag{21}$$

Expressions specific to the case with leakage

Since even numerical evaluation of the integral for the symbol error probability in (8) is difficult in general, a different strategy was taken. An upper bound on $Q_1(a,b)$ yields a upper bound on the probability of making a symbol error in Eq. (22), and similarly a lower bound on $Q_1(a,b)$ will yield a lower bound on the symbol error probability. The upper bound expression is given by [9]:

$$P_{upper}(E) = 1 - \frac{1}{2\sigma^2}\int_0^\infty \exp\left[-\frac{y+s^2}{2\sigma^2}\right] I_0\left(\frac{s\sqrt{y}}{\sigma^2}\right)\left(1-\exp\left(-\frac{\left(\sqrt{y}-s_L\right)^2}{2\sigma^2}\right)\right)^{M-1} dy \tag{22}$$

Similarly, the lower bound expression is:

$$P_{lower}(E) = 1 - \frac{1}{2\sigma^2}\int_0^\infty \exp\left[-\frac{y+s^2}{2\sigma^2}\right] I_0\left(\frac{s\sqrt{y}}{\sigma^2}\right)\left(1-\exp\left(-\frac{\left(\sqrt{y}+s_L\right)^2}{2\sigma^2}\right)\right)^{M-1} dy \tag{23}$$

The bounds on SER given by Eqs. (22) and (23) were evaluated via numerical integration using measured values of the following three parameters:

1. s^2: The sum of the squared means of the matched filter outputs in a signal slot.
2. s_L^2: The sum of the squared means of the matched filter outputs in a noise slot.
3. σ^2: The variance of the matched filter real and imaginary parts. Since the real and imaginary parts each have variance σ^2, the total variance of the complex Gaussian matched filter output is $2\sigma^2$.

The three parameters above must be estimated from the experimental data since the leakage is unknown *a priori*.

Computing Bit Error Rate of Non-Coherent Detection of M-ary Orthogonal Signal in the Presence of Gaussian Noise with Non-Zero Mean Using Saddle-Point Approximation

In the previous section, simpler upper and lower bounds of Eq. (8) were analyzed, but these bounds are loose for the high signal-to-noise ratio region Another approach to solve for Eq. (8). In this section the objective is to evaluate the Saddle-Point approximation of the Marcum-Q function which in turn provides a simplified yet tight approximation of the BER expression of Eq. (8).

The Marcum-Q function is given by the following expression

$$Q_1(a,b) = \int_b^\infty x e^{-\frac{x^2+a^2}{2}} I_0(ax)dx\,. \tag{24}$$

Then if we define:

$$f(x) = x e^{-\frac{x^2+a^2}{2}} I_0(ax)\,, \tag{25}$$

$$g(x) = \log_e f(x) \tag{26}$$

We need to find x_m such that $f(x_m)$ is maximized, we evaluate the derivative of $f(x)$ as:

$$f'(x) = e^{-\frac{x^2+a^2}{2}}((1-x^2)I_0(ax) + axI_1(ax)) \tag{27}$$

Then we define

$$h(x) = (1-x^2)I_0(ax) + axI_1(ax) \tag{28}$$

We evaluate the derivative of $h(x)$ as

$$h'(x) = x(-2+a^2)I_0(ax) + a(1-x^2)I_1(ax) \tag{29}$$

x_m can be found iteratively using Newton's Method of

$$x_{i+1} = x_i + \frac{h(x_i)}{h'(x_i)}, \qquad i = 0,1,2,... \tag{30}$$

It can be shown that a good choice of initial value x_0 is given by the following expression

$$x_0 = \sqrt{\frac{\pi}{2}} e^{-\frac{a^2}{4}}((1+\frac{a^2}{2})I_0(\frac{a^2}{4}) + \frac{a^2}{2}I_1(\frac{a^2}{4})), \tag{31}$$

particularly when a is large, and $x_i \to x_m$ after a few iterations.

Next we evaluate the first and second derivatives of $g(x)$ as follows:

$$g'(x) = \frac{1}{x} - x + \frac{aI_1(ax)}{I_0(ax)} \tag{32}$$

$$g''(x) = \frac{1}{2}(-2 + a^2 - \frac{2}{x^2} + a^2 \frac{-2I_1(ax)^2 + I_0(ax)I_2(ax)}{I_0(ax)^2}) \tag{33}$$

The Saddle-Point approximation $Q_1*(a,b)$ of $Q_1(a,b)$ is given by

$$Q_1*(a,b) = \int_b^\infty f(x_m) e^{\frac{g''(x_m)(x-x_m)^2}{2}} dx, \tag{34}$$

where $f(x)$ and $g''(x)$ are defined in equations (25) and (33) respectively, and x_m is evaluated using the iterative procedure as described in (a7) and (a8). Thus we show that the Marcum-Q function can be

approximated by a definite integral of an un-normalized Gaussian as shown in (a11). This approximation is particularly good when b , which denote the signal-to-noise ratio, is reasonably large.

The saddle point approximation will allow us to replace the integral from Eq. (8) with the following integral:

$$P(E)=1-\frac{1}{2\sigma^2}\int_0^\infty \exp\left[-\frac{y+s^2}{2\sigma^2}\right]I_0\left(\frac{s\sqrt{y}}{\sigma^2}\right)\left(1-Q_1^*\left(\frac{s_L}{\sigma},\frac{\sqrt{y}}{\sigma}\right)\right)^{M-1}dy \tag{35}$$

replacing the Marcum-Q function with its saddle point approximation.

Now we can write the approximation to the Marcum-Q function as:

$$Q_1^*(a,b)=\frac{\sqrt{\pi}}{2}\sqrt{-\frac{2}{g''(x_m)}}f(x_m)\operatorname{erfc}\left((b-x_m)\sqrt{-\frac{g''(x_m)}{2}}\right) \tag{36}$$

where it is understood that x_m is a function of a .

We substitute equation (36) into equation (37) in order to obtain a new integral shown in Eq. (37):

$$P(E)=1-\frac{\left[\frac{\sqrt{\pi}}{2}\sqrt{-\frac{2}{g''(x_m)}}f(x_m)\right]^{M-1}}{2\sigma^2}\int_0^\infty\left[\exp\left[-\frac{y+s^2}{2\sigma^2}\right]I_0\left(\frac{s\sqrt{y}}{\sigma^2}\right)\left(\operatorname{erfc}\left(\left(\frac{\sqrt{y}}{\sigma}-x_m\right)\sqrt{-\frac{g''(x_m)}{2}}\right)\right)^{M-1}\right]dy \tag{37}$$

4. Results of the Coherent Optical Receiver Experiment (CORE)

The experimental setup [1, 9] consists of two Nd:YAG (YAG denotes yttrium aluminum garnet) lasers operating at 1064 nm, whose outputs are aligned and combined on the surface of a 4 X 4 Fermionics InGaAs detector array. One of the lasers serves as a local oscillator, while the other simulates the received signal. The two lasers are operated at slightly different wavelengths, yielding a relatively stable difference-frequency tone of approximately 6 MHz in the detected signal. In the presence of spatial distortions simulating atmospheric turbulence conditions, the difference-frequency tone is generally observable in several array elements simultaneously, but usually with different phases. In the current coherent combining experiment, each of the 16 outputs of the detector array is amplified, and input to a 16-channel data-acquisition assembly (using GaGe data-acquisition cards). The analog signals are digitized to 8 bits at a sampling rate of 25 megasamples per second (MSPS). The modulation format for the transmitted laser signal is PPM using an external Electro-Optic Modulator (Pockle cell). The resulting sample stream acquired with the GageScope is digitally downconverted to complex baseband. The resulting downconverted complex samples served as input to a least-mean-square (LMS) algorithm, which was used to estimate the complex weights required to reconstruct the signal. The complex-weighted samples from each channel were then combined, in order to maximize the combined signal-to-noise ratio (SNR). A rotating predistorted plexiglass plate was incorporated into the experimental setup to simulate atmospheric turbulence.

Figure 1 is a photograph of the optical setup at the Jet Propulsion Laboratory where the experiments described in this thesis have taken place. This signal laser beam is focused into the photodetector via the receiver lens.

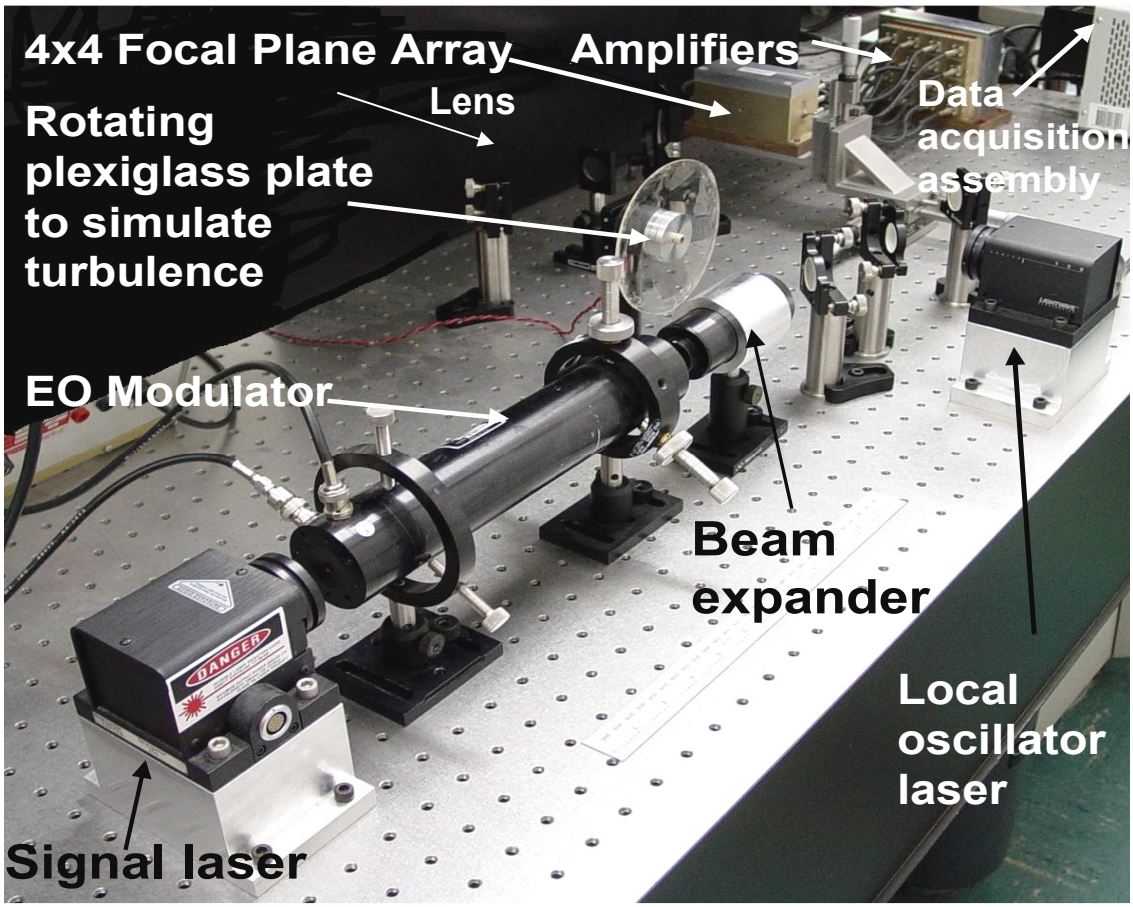

Figure 1. Coherent combining experiment at the Jet Propulsion Laboratory, NASA.

Evaluation of experimental system performance and comparison with theory

A brief summary of the results will be shown in this section as it was already published in [1]. In Figure 2, BER is plotted against photons per bit BER for the case of 256 PPM for a single detector configuration. The experimental points lie close to the theoretical BER performance line, and the trend line fitted to the experimental points is seen to lie very close to the theoretical bound. This figure shows a bit error rate only slightly above $3 \cdot 10^{-3}$ at 1 photon per bit, illustrating the system's performance in the presence of weak signals. Figure (3) shows the computation of hypothetical FPA performance if the detector elements had the same characteristics as the single detector.

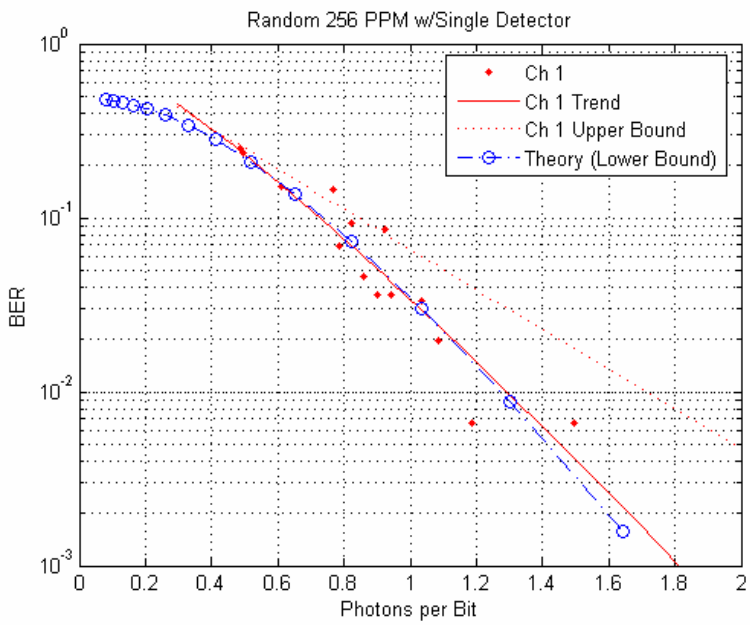

Figure 2. BER vs. photons per bit with the single detector and 256 PPM.

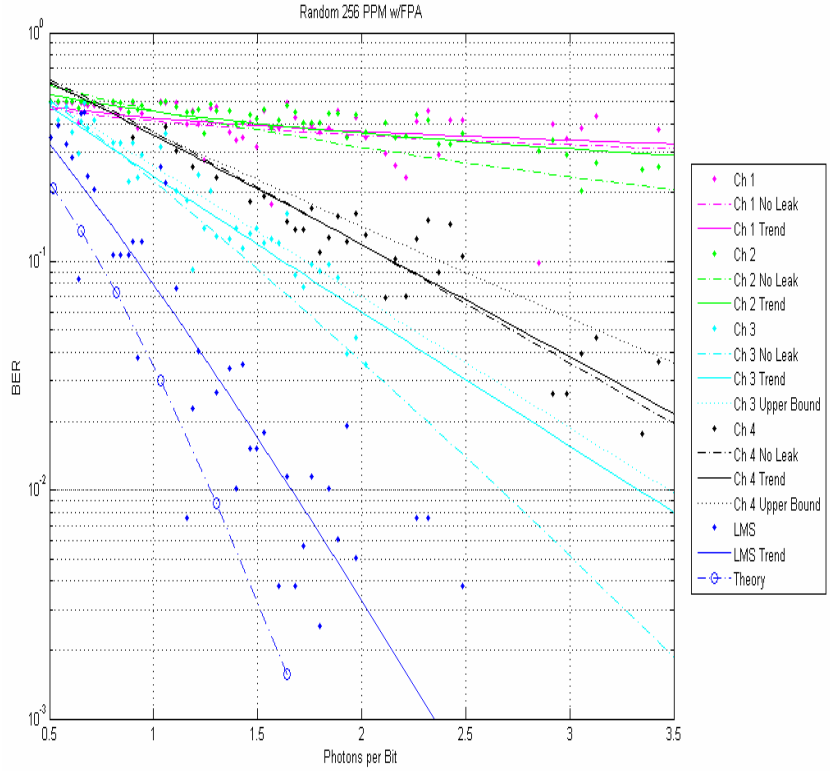

Figure 3. BER vs. photons per bit with the single detector and 256 PPM.

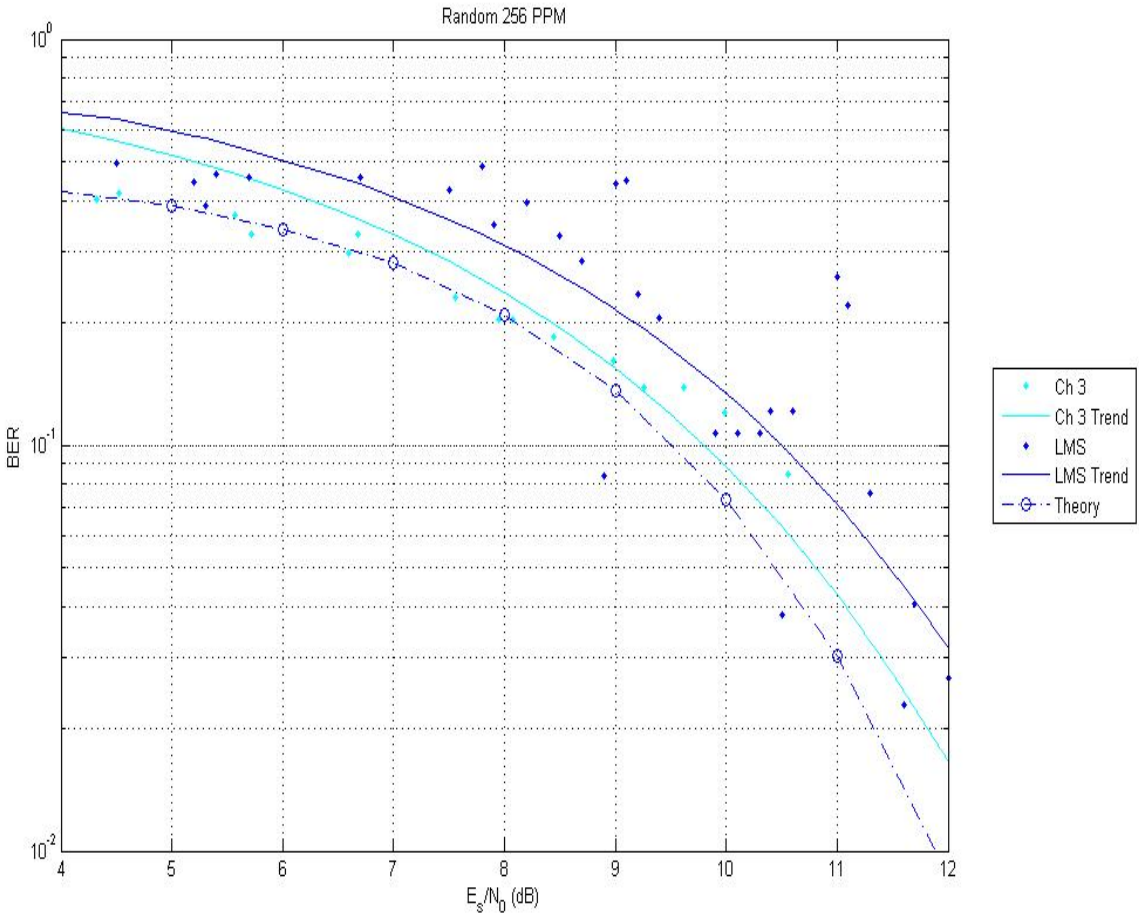

Figure 4. BER vs. Es/N0 for 256 PPM: Illustration of single channel performance vs. combined channel. Single channel BER is plotted vs. single channel SNR.

Figure (4) shows BER as a function of SNR for 256 PPM. Performance of a single channel (channel 3) is compared to that of the combined channel. It is important to notice that single channel BER is plotted vs. individual channel SNR and not against combined channel SNR as in the previous figure. One observes a 0.2 dB loss due to the leakage term in channel 3 illustrated by the horizontal difference between the theoretical (blue-dotted curve) and the experimental channel 3 curve (cyan). The combining loss for this case is 0.8 dB when comparing the experimental channel 3 curve with the experimental combined channel curve (continuous blue curve).

In summary, high quality low noise receiver electronics and/or a sufficiently powerful local oscillator laser operating at or near the shot noise limit, used in conjunction with a focal plane array, will enable bit error rate performance close to that achievable in the absence of atmospheric turbulence. Again, combined channel performance is within less than 0.5 photons per bit of the theoretical performance curve, indicating that much of the signal energy scattered across the five FPA elements used in combining can be recovered. These results, like those for 256 PPM, indicate that coherently combining the outputs of the FPA channels permits very good reconstruction of the signal that would have existed if no turbulence had been present and if all photons had been hitting this detector.

5. Conclusions and future directions

The results presented here are highly promising, and there are many very productive directions for future research. Future work includes to plot the resulting BER approximation curve from Eq. (37) with the curve from measurement, upper bound and lower bound and compare those results with the main results obtained in this paper. Then, one could investigate how this result can apply to mobile communication scenarios to estimate BER of Rician channels.

.

Coherent combining algorithms for focal plane arrays are an area of further research. In a realistic space communications system utilizing PPM, the relative positions of the spacecraft and the ground receiver may change by many optical wavelengths between PPM pulses. Since no signal exists during the inter-pulse intervals, tracking of the spacecraft signal phase poses a challenge under some operating conditions, depending on the degree of pulse-to-pulse phase coherence present.

The use of coding would unleash the true potential of the focal plane array receiver. Uncoded bit error rates below 10^{-1} are achievable using a shot-noise-limited receiver running at slightly less than one photon per bit. Corresponding coded bit error rates would be significantly lower, enabling very robust digital communications at low signal levels. The ability to communicate reliably at such weak signal levels would greatly extend the utility and usefulness of optical communications for deep space, especially in light of the severe demands generated by deep space link budgets.

REFERENCES

1. M. Muñoz Fernández, V. A. Vilnrotter, R. Mukai, and Babak Hassibi, *Coherent Optical Array Receiver Experiment: Design, Implementation and BER Performance of a Multichannel Coherent Optical Receiver for PPM Signals under Atmospheric Turbulence.* Proc. of *SPIE Vol. 6105R, (2006), Free-Space Communication Technologies XVIII, ed. by G. Stephen Mecherle.*

2. R. M. Gagliardi, S. Karp, *Optical Communications*, 2nd ed., Wiley Series in Telecommunications and Signal Processing, New York, 1995, Chapter 6.

3. Larry C. Andrews, University of Central Florida, *Field Guide to Atmospheric Optics,* SPIE Field Guides, Volume FG02, John E. Greivenkamp, Series Editor, SPIE Press,Washington 2004.

4. J. W. Goodman. 2005. *Introduction to Fourier Optics*. Englewood, Colorado: Roberts & Co.

5. S. Zohar, and V. Vilnrotter, ``Using a Focal-Plane Array to Estimate Antenna Pointing Errors," *JPL External Publication 91-45*, October 1991.

6. M. K. Simon, S. Hinedi, and W. Lindsey. 1995. *Digital Communication Techniques, Signal Design and Detection.* Upper Saddle River, New Jersey: PTR Prentice Hall.

7. V. A. Vilnrotter, Rodemich, E.R.; Dolinar, S.J., Jr. March 1992. "Real-time combining of residual carrier array signals using ML weight estimates." *IEEE Transactions on Communications*, vol. 40, n. 3, pp. 604–615.

8. M. K. Simon. 2002. Probability Distributions Involving Gaussian Random Variables, A Handbook for Engineers and Scientists. Norwell, Massachusetts: Kluwer Academic Publishers.

9. Michela Muñoz Fernández, Coherent Optical Array Receiver For PPM Signals Under Atmospheric Turbulence, Ph.D. Thesis, Dept. of Electrical Engineering, California Institute of Technology, 2006.

National Aeronautics and
Space Administration

Jet Propulsion Laboratory
California Institute of Technology
Pasadena, California

Coherent Optical Focal Plane Array Receiver for PPM Signals: Investigation and Applications

MICHELA MUÑOZ FERNÁNDEZ

Aug. 15, 2006

SPIE Optics and Photonics 2006

Outline

- Introduction
  - Contributions
- Laser communications for deep space
- CORE: Coherent Optical Receiver Experiment
- Analytical expression to evaluate BER
- Adaptive Signal Processing with LMS
- Experimental Setup
- Experimental Results
- Summary and Conclusions

Introduction

- ***Contributions***

- ***First time an optical coherent (heterodyne) focal plane array receiver for PPM signals has been designed and implemented for deep space communications that is capable of compensating for atmospheric turbulence distortions and able to work under high background noise levels***

  – ***Demonstration of signal array combining gain by means of LMS algorithm for an optical coherent receiver***

    - ***Compensate for atmospheric turbulence***
    - ***Used with 256-PPM signals in the context of deep space optical communications***
    - ***Use of constant target LMS (no need for a reference signal)***
    - ***Demonstration of the potential for shot noise limited performance with a focal plane array (FPA)***

Shot noise limited performance-CORE

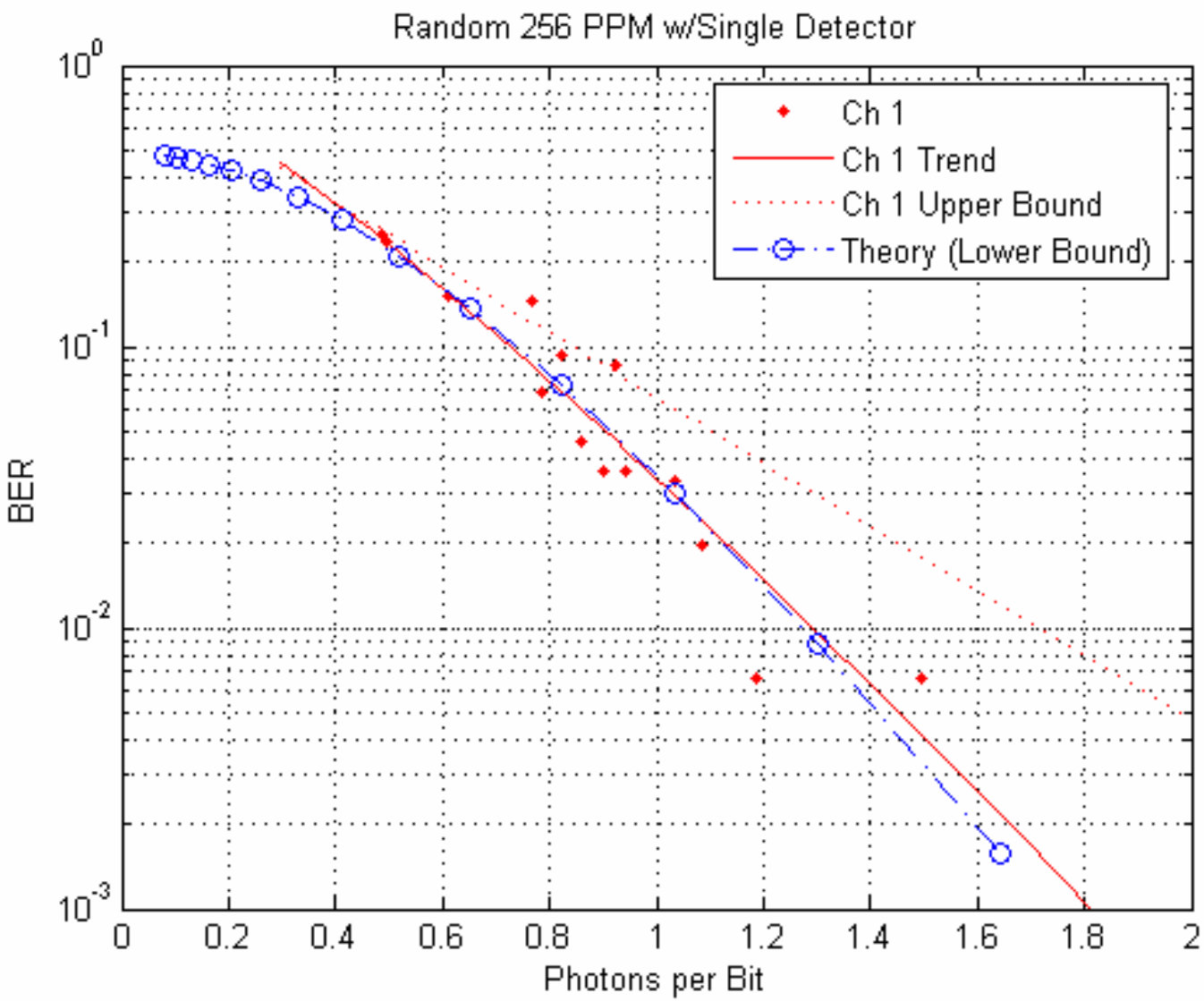

Advantages of laser over RF communications

Future interplanetary missions needs: higher capability and smaller and more efficient space-borne telecommunications

- Ability to concentrate power in narrower beams (small beam divergence)
- Higher frequencies: higher transmission bandwidth : higher information capacity of the system
- Transmitters and receivers are smaller and lighter
- Higher security and greater resistance to interference
- Spectrum for laser communications not regulated yet

Laser communications terminology

- **Definitions**
  - Optically coherent: Refers to any laser communications system that uses optical signal mixing
  - Optically non-coherent: Refers to direct direction optical systems
  - Coherent: Refers to a communications system that requires carrier recovery
  - Non-coherent: Refers to a communications system that operates without carrier recovery
- The system implemented in this thesis is based on an optically coherent heterodyne receiver, but with non-coherent demodulation

Laser communications for deep space

- ***Advantages of optically coherent vs. direct detection***
  - Superior sensitivity under ideal conditions when signal strength is limited
  - More immune to background noise- allows operation of S/C close to the Sun
  - Frequency selectivity
- ***Disadvantages of optically coherent vs. direct detection***
  - Sensitive to optical alignment issues
  - Requires high stability lasers

Laser communications for deep space

- ***Problems due to atmospheric turbulence***
- Problems arise when using optical communications due to short optical wavelengths; terrestrial reception suffers from clear-air turbulence and cloud absorption effects that do not plague longer-wavelength RF systems (clear-air turbulence problem addressed here)
- Laser communications performance is affected by the atmosphere as it is a dynamic and imperfect medium
- Atmospheric channel effects include fluctuations in the signal amplitude, phase, and attenuation

- ***Solution proposed***
  - *The solution proposed here is to use focal-plane arrays to collect the optical signals from different spatial modes of the received signal field simultaneously, and then recombine the signals adaptively*

Transmitter technologies

LASER TYPE	EXAMPLES	OPEARATING WAVELENGTHS	DRAWBACKS
Semiconductor	AlGaAs InGaAsP	830 nm 980 nm 1550 nm	Low powers
Solid State	Nd:YAG	1060 nm	Separate modulator
Gas	CO_2 HeNe	10,600 nm 530 nm	Complexity Lifetime issues
Fiber	Erbium doped fiber	1550 nm	Not tested in space environment

Pulse Position Modulation

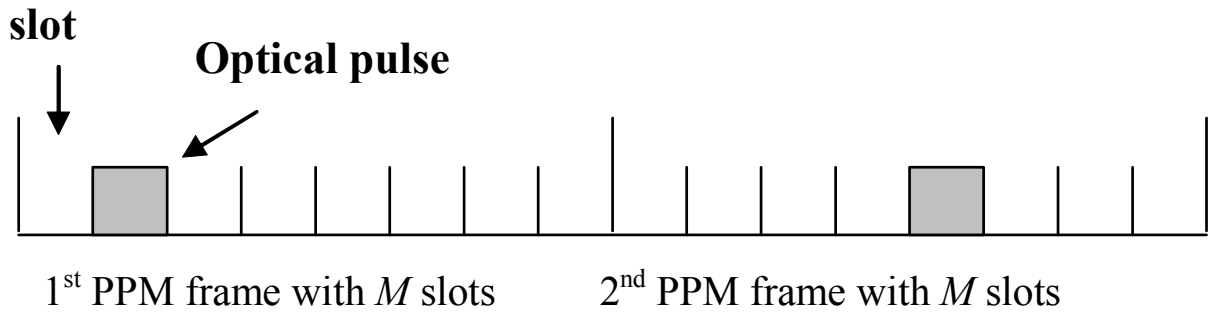

- PPM was selected by JPL for use with direct detection receivers. Our choice of PPM was to be compatible with existing PPM systems.

-Capacity (in bits per photon or bits per channel use) is not bounded for noiseless PPM, if perfect timing is assumed

-Capacity in bits per photon (or bits per channel use) increases as $\log_2 M$, an unbounded number as M increases.

CORE: Coherent Optical Receiver Experiment

- Channel
  - Free space:
    - Clear air turbulence channel
    - Link from Deep Space to Earth

- **Receiver**
  - Optically coherent heterodyne
  - Demodulation: non-coherent

- The receiver decides on the basis of maximum likelihood symbol detection; it selects the slot with the greatest energy and the symbol that contains a signal pulse in that slot location is declared to be the transmitted symbol

  - Detector: InGaAs PIN diode
  - Array configuration: focal plane array of InGaAs PIN diode detectors
  - Evaluation of performance based on receiver sensitivity given by BER as a function of photons/bit

CORE: Coherent Optical Receiver Experiment

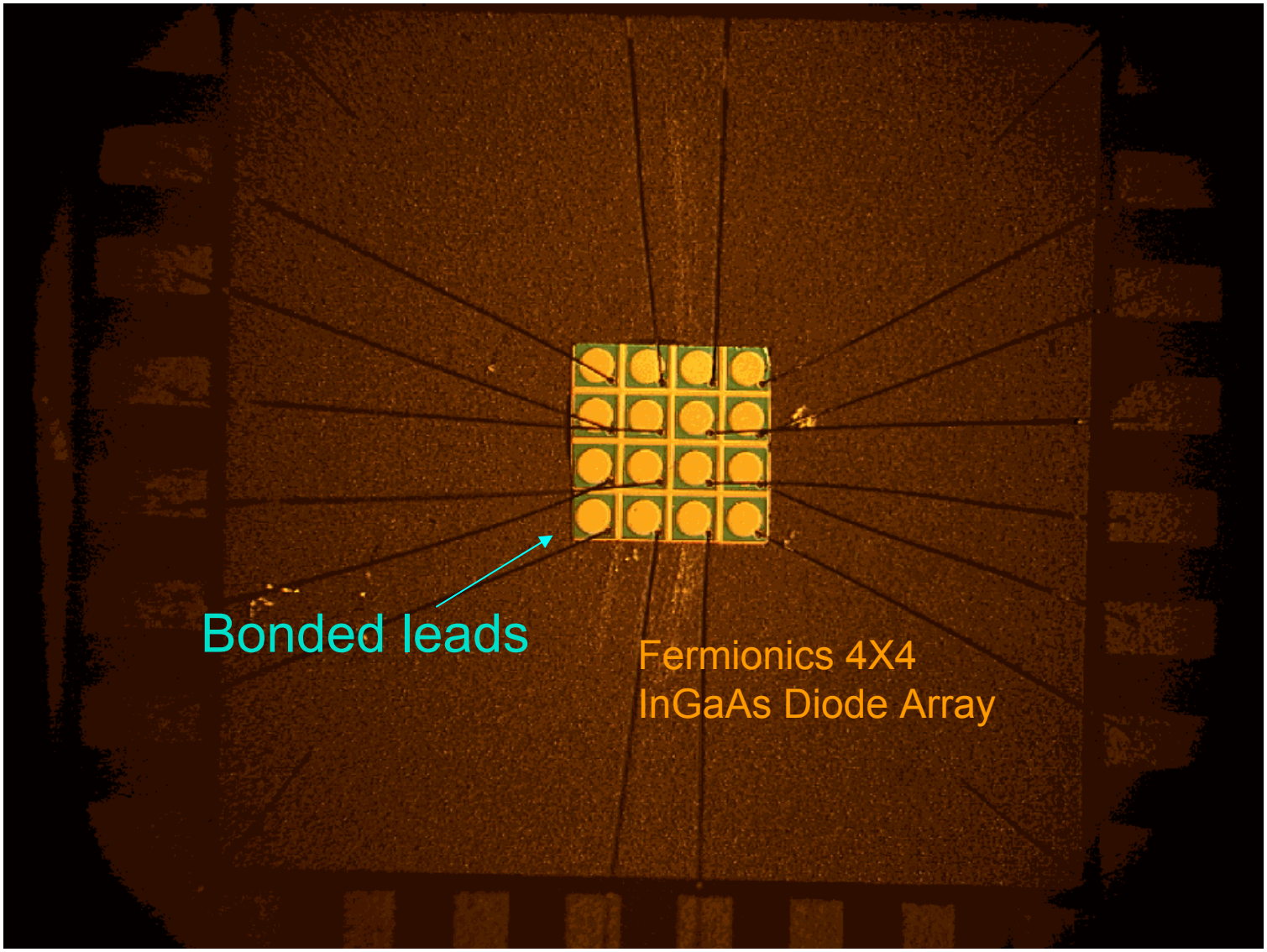

CORE: Coherent Optical Receiver Experiment

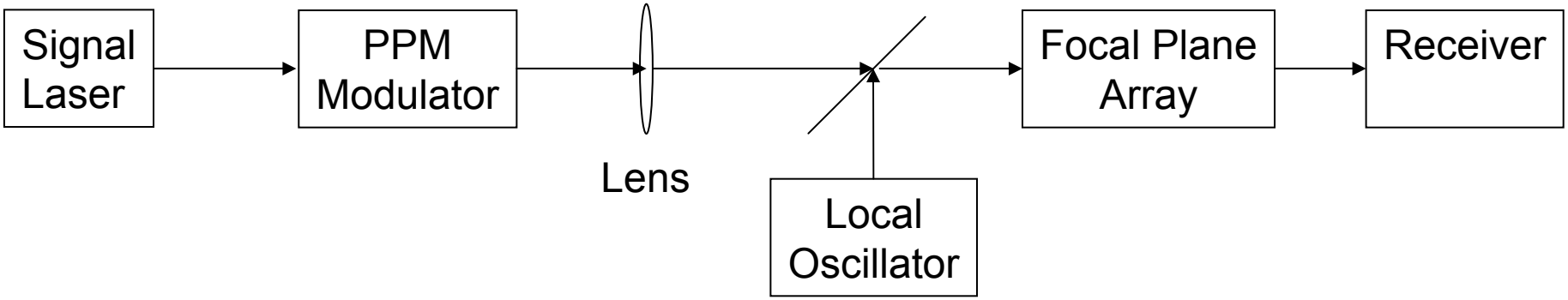

CORE: Coherent Optical Receiver Experiment

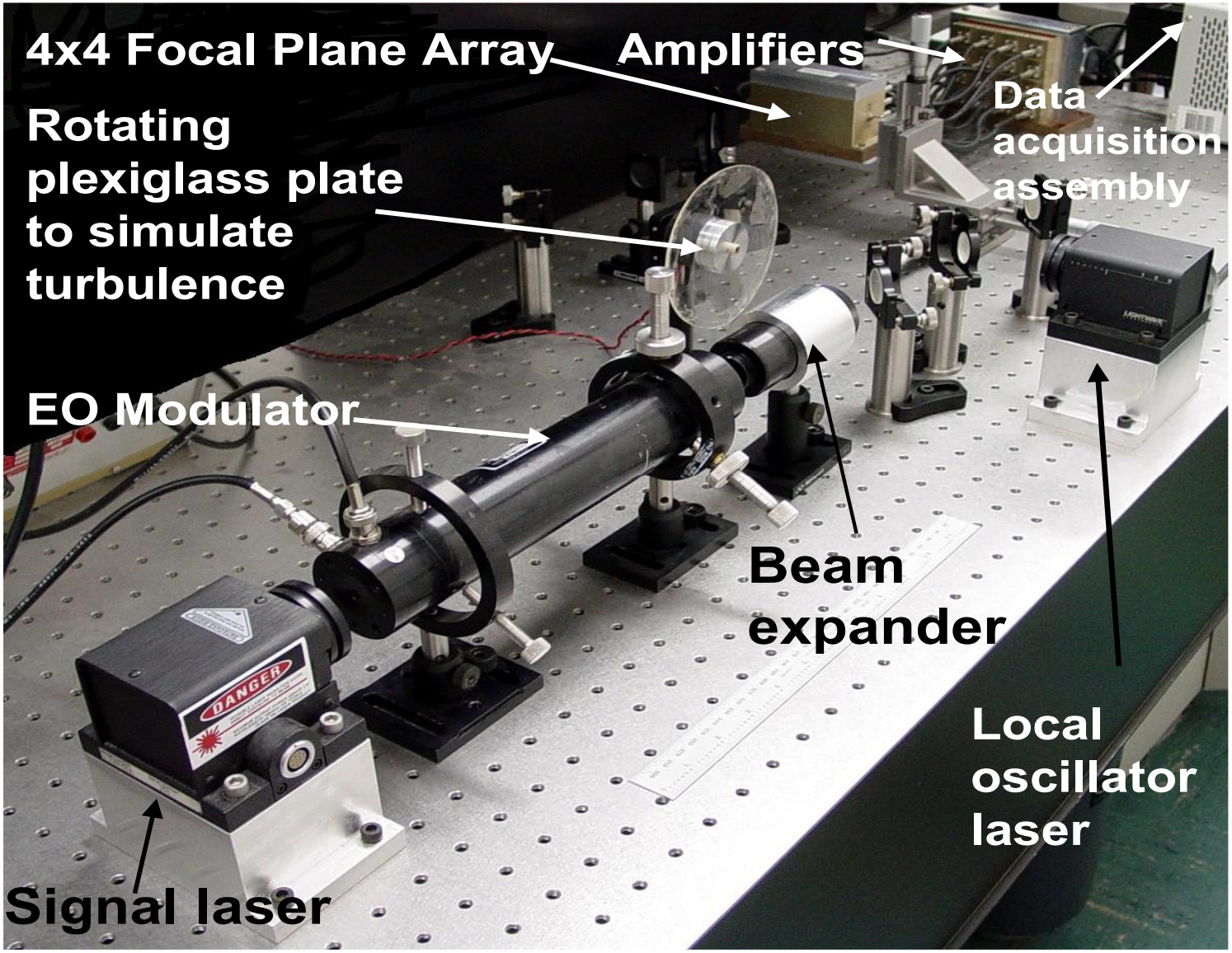

Optically Coherent Receiver Theory

•Beam-splitter spatially combines the carrier with an unmodulated laser local oscillator beam whose frequency differs by the desired IF

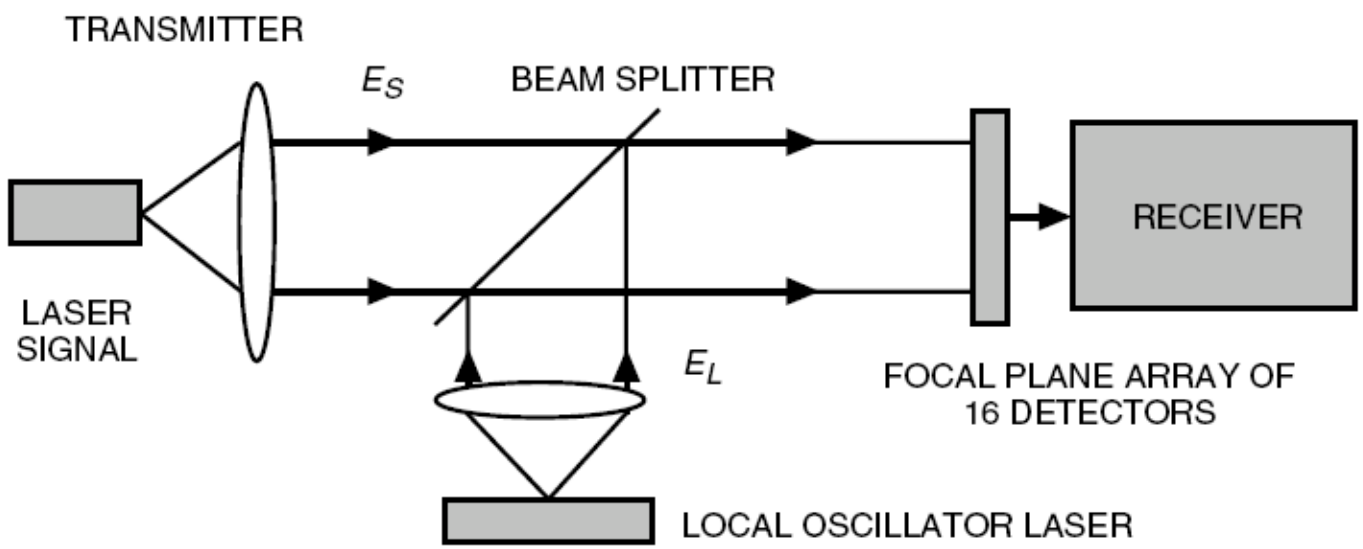

$$a_{\mathbf{R}}(t) = s(t) + b(t)$$

$$I(t) = \left|a_{\mathbf{R}}(t)\right|^2 + \left|a_L\right|^2 + 2\left|a_L\right|\left|a_{\mathbf{R}}(t)\right|\cos\left[\left(\omega_s - \omega_L\right)t + \theta_{\mathbf{R}}(t) - \theta_L\right],$$

Calculation of Signal to Noise ratio for heterodyne detection

Energy per symbol $E_s = 2(e\alpha)^2 P_s P_L T_s,$

Noise spectral density $N_0 = e^2[\alpha P_L + \alpha^2 P_L N_{0b}] + N_{th},$

Heterodyned SNR $$\frac{E_s}{N_0} = \left[\frac{2\alpha P_s T_s}{1 + \alpha N_{0b} + \left(N_{th} / \alpha P_L e^2\right)}\right]$$

Assuming shot noise limited conditions $\alpha P_L \gg N_{th} / e^2$

And with $K_s = \alpha P_s T_s$ $\Rightarrow$ $$\frac{E_s}{N_0} = \left[\frac{2K_s}{1 + \alpha N_{0b}}\right]$$

Assuming negligible background noise

$$\frac{E_s}{N_0} = 2K_s$$

$\alpha = \eta_q / h\nu$ $\quad QE = \eta_q = \frac{Rh\nu}{e}$

Noncoherent Receiver

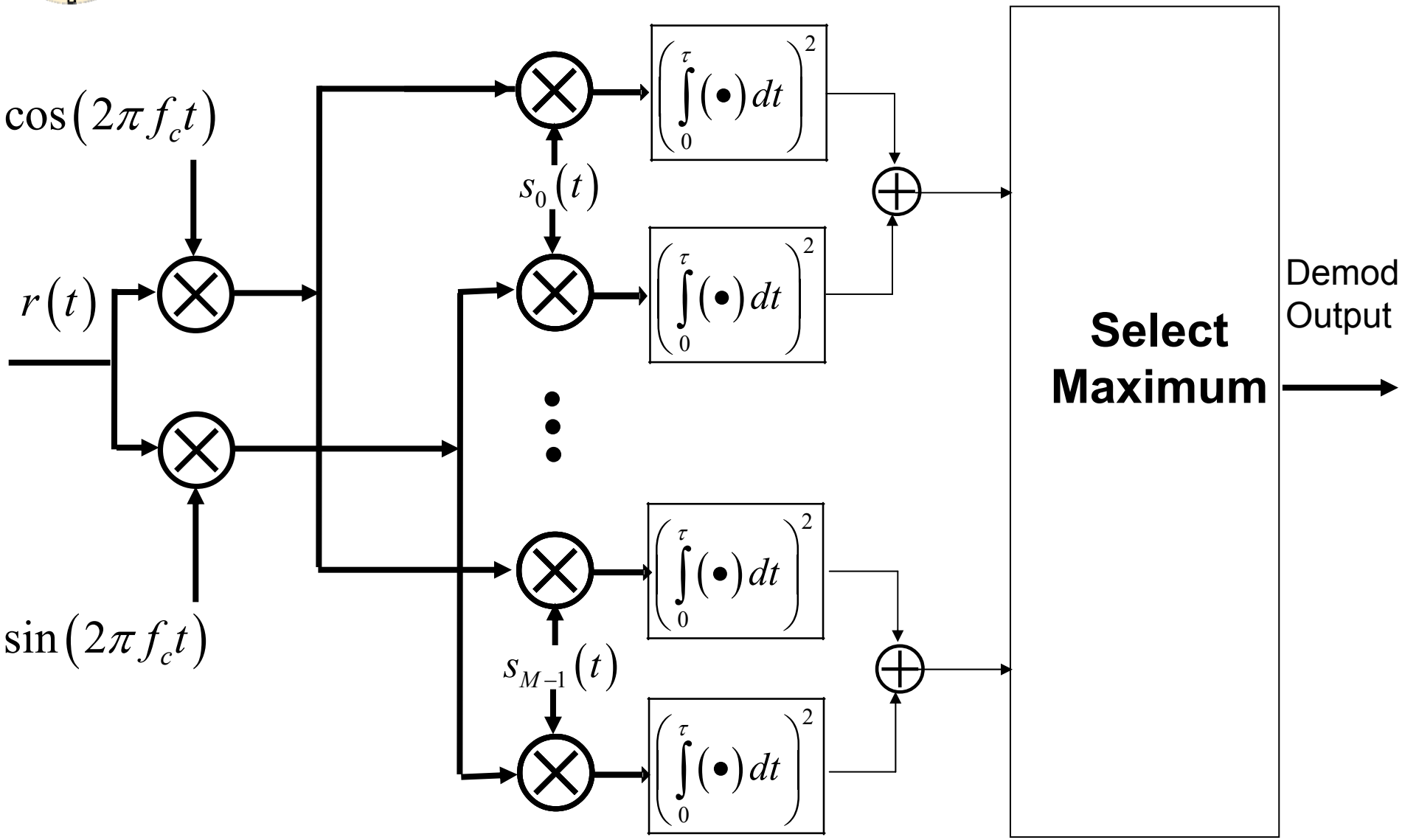

BER Expressions for heterodyne detection

-Non-coherent receiver (Simon, 1995)

$$P_b(E) = \frac{M/2}{M-1} \sum_{m=1}^{M-1} (-1)^{m+1} \frac{1}{m+1} {}_{M-1}C_m \exp\left\{ -\frac{m}{m+1} \left(\frac{E_s}{N_0} \right) \right\}$$

where $${}_{M-1}C_m = \frac{(M-1)!}{m!(M-1)!}$$

- Array with AWGN and optimal combining (Vilnrotter, Rodemich)

$$\left(\frac{E_S}{N_0} \right)_{total} = \sum_{i=1}^{N} \left(\frac{E_S}{N_0} \right)_i$$

Leakage Case: Definitions

•Due to imperfections in the modulator there is an unwanted signal component present in the noise slots that from now on is referred to as “leakage”

- Definitions
  - x_1 : The real part of the matched filter output
  - x_2 : The imaginary part of the matched filter output
  - m_1 : $E[x_1]$
  - m_2: $E[x_2]$
  - σ^2: $\mathrm{Var}[x_1] = \mathrm{Var}[x_2]$ (signal and noise slots)
  - s^2 : $m_1^2 + m_2^2$ in a signal slot
  - s_L^2 : $m_1^2 + m_2^2$ in a noise slot

Expressions for SNR and BER

(Simon, 1995, 2004)

$$\mathrm{SNR} = 10\log_{10}\left(\frac{E_S}{N_0}\right) = 10\log_{10}\left(\frac{s^2}{2\sigma^2}\right)$$

$$\mathrm{BER} = \left(\frac{M/2}{M-1}\right)\left(1 - \frac{1}{2\sigma^2}\int_0^\infty \exp\left(-\frac{y+s^2}{2\sigma^2}\right)\mathrm{I}_0\left(\frac{s}{\sigma^2}\sqrt{y}\right)\left(1 - Q_1\left(\frac{s_L}{\sigma}, \frac{\sqrt{y}}{\sigma}\right)\right)^{M-1} dy\right)$$

$$\mathrm{BER} \le \left(\frac{M/2}{M-1}\right)\left(1 - \frac{1}{2\sigma^2}\int_0^\infty \exp\left(-\frac{y+s^2}{2\sigma^2}\right)\mathrm{I}_0\left(\frac{s}{\sigma^2}\sqrt{y}\right)\left(1 - \exp\left(-\frac{\left(\sqrt{y}-s_L\right)^2}{2\sigma^2}\right)\right)^{M-1} dy\right)$$

$$\mathrm{BER} \ge \left(\frac{M/2}{M-1}\right)\left(1 - \frac{1}{2\sigma^2}\int_0^\infty \exp\left(-\frac{y+s^2}{2\sigma^2}\right)\mathrm{I}_0\left(\frac{s}{\sigma^2}\sqrt{y}\right)\left(1 - \exp\left(-\frac{\left(\sqrt{y}+s_L\right)^2}{2\sigma^2}\right)\right)^{M-1} dy\right)$$

The upper and lower bounds given above will be mathematically equal to each other and to the non-leakage expression for BER whenever $s_L = 0$, which is the case without leakage. Hence, the leakage case reduces to the no leakage case as expected.

Experimental Setup

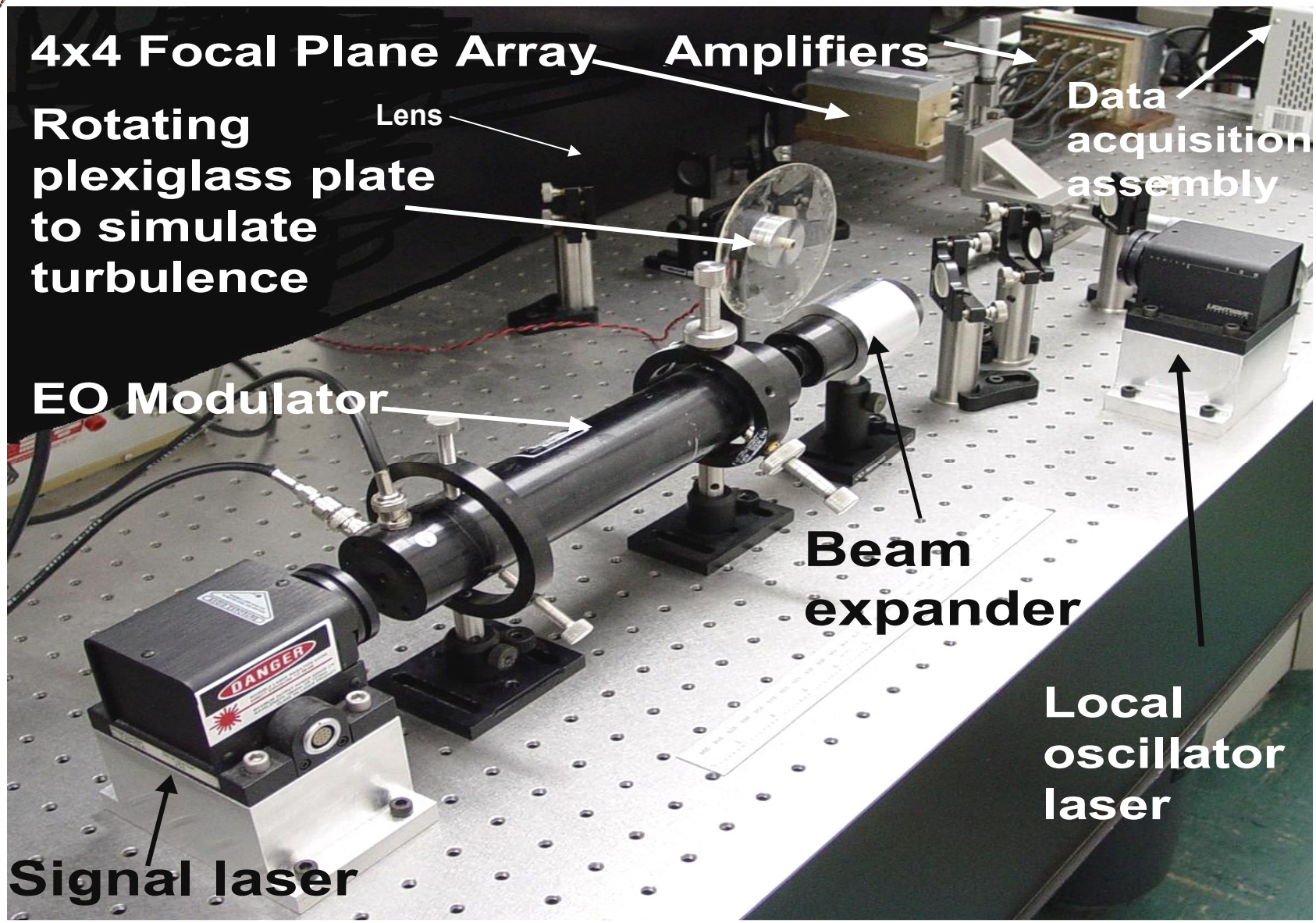

Experimental Setup

- Developed Digital Data Acquisition and Post-detection Signal Processing System
- Obtained sampled outputs of the 16 channels using Gage Scope Data Acquisition Assembly at 25 MSPS

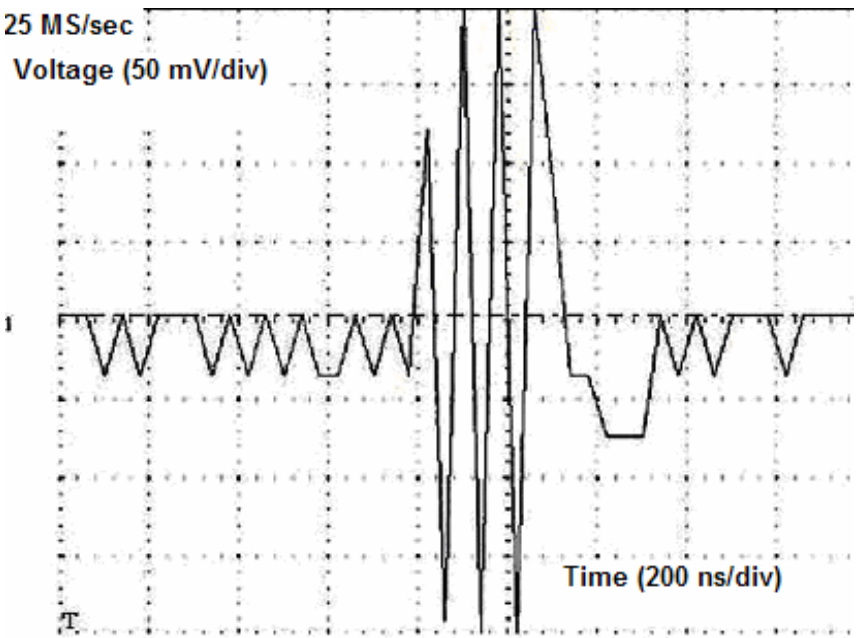

Experimental Setup

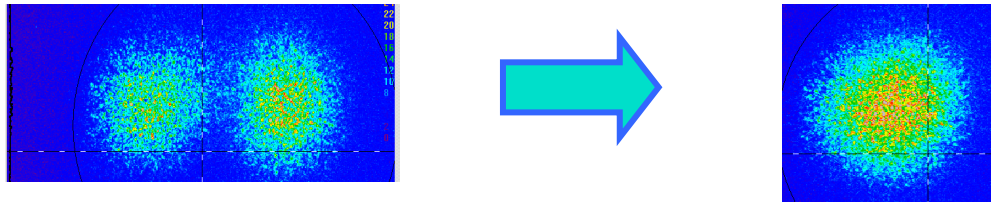

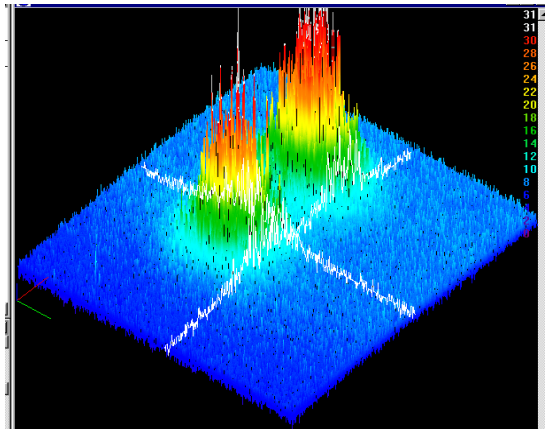

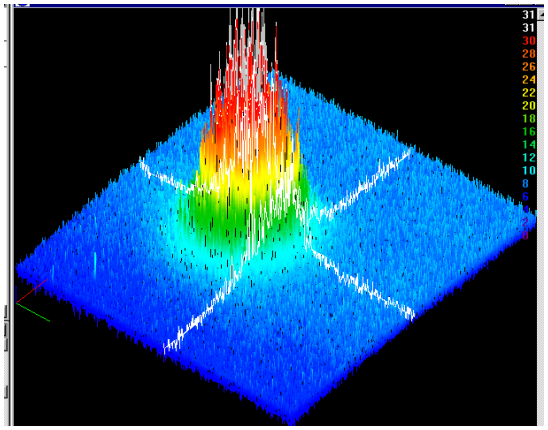

Experimental Setup

•Obtained intensity distributions of signal beam at the input to the focal-plane array with and without simulated turbulence

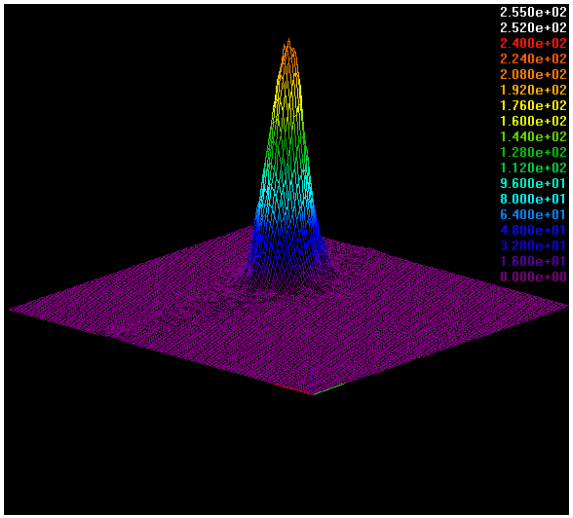

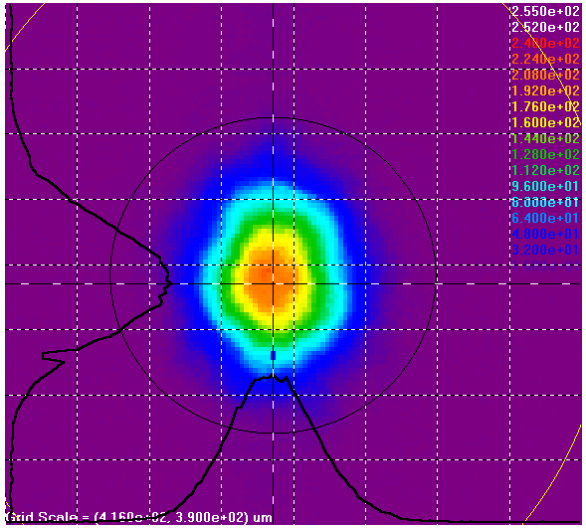

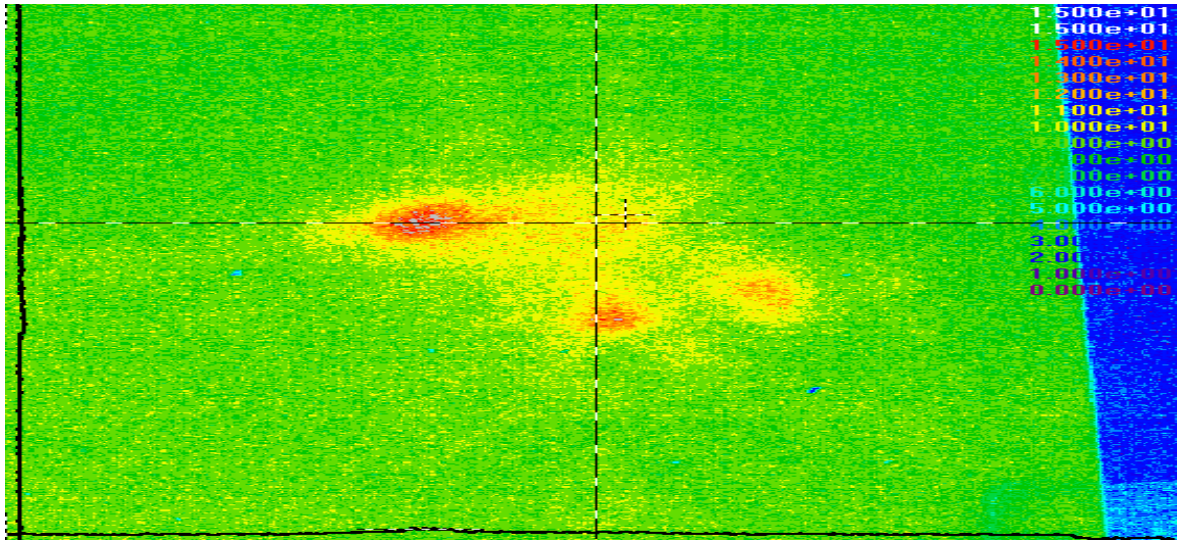

Experimental results

- The optical local oscillator frequency was displaced from the received optical signal frequency by 6 MHz, resulting in an intermediate detected frequency of 6 MHz.
- The heterodyned PPM intermediate signal was sampled at 25 MHz (40 ns samples), and the resulting sample-stream digitally downconverted to complex baseband.
- The resulting downconverted complex samples served as input to a least-mean-square (LMS) algorithm, which was used to estimate the complex weights required to reconstruct the signal.

Adaptive Combining with LMS

- Received signal

$$\mathbf{r}(k) = \mathbf{s}(k) + \mathbf{n}(k)$$

- The output of the linear combiner is

$$y(k) = \mathbf{w}^H(k)\mathbf{r}(k)$$

- The goal is to minimize the mean squared error (MSE)

$$\mathrm{MSE}(k) = E\left[\left|d(k) - y(k)\right|^2\right]$$

LMS with Decision Feedback

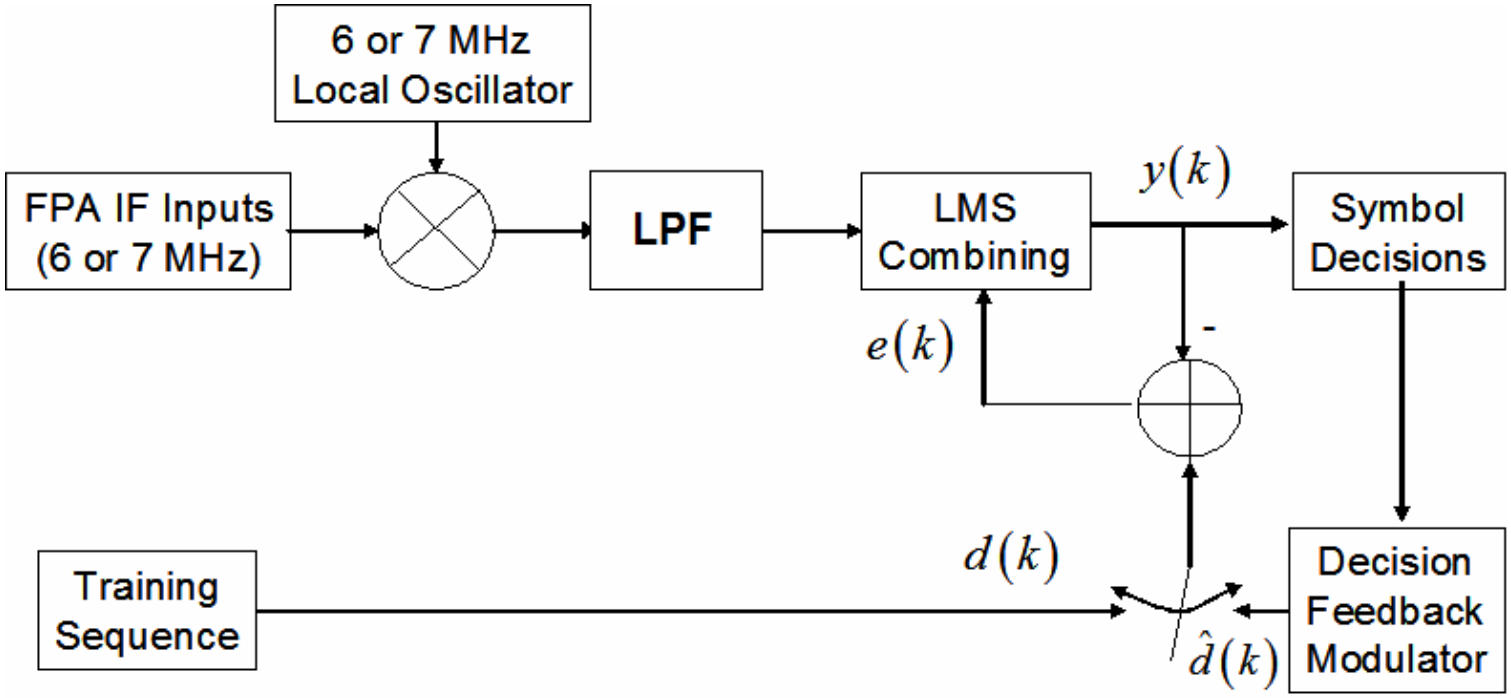

$$\mathbf{w}(k+1) = \mathbf{w}(k) + \mu e^*(k)\mathbf{r}(k)$$

$$\text{where } e(k) = \begin{cases} d(k) - y(k) = d(k) - \mathbf{w}(k)^H \mathbf{r}(k) & \text{acquisition} \\ \hat{d}(k) - y(k) = \hat{d}(k) - \mathbf{w}(k)^H \mathbf{r}(k) & \text{tracking (decison feedback)} \end{cases}$$

LMS Convergence

$$\mu = 10 \qquad \mu_{\max} = 1.53 \cdot 10^3$$

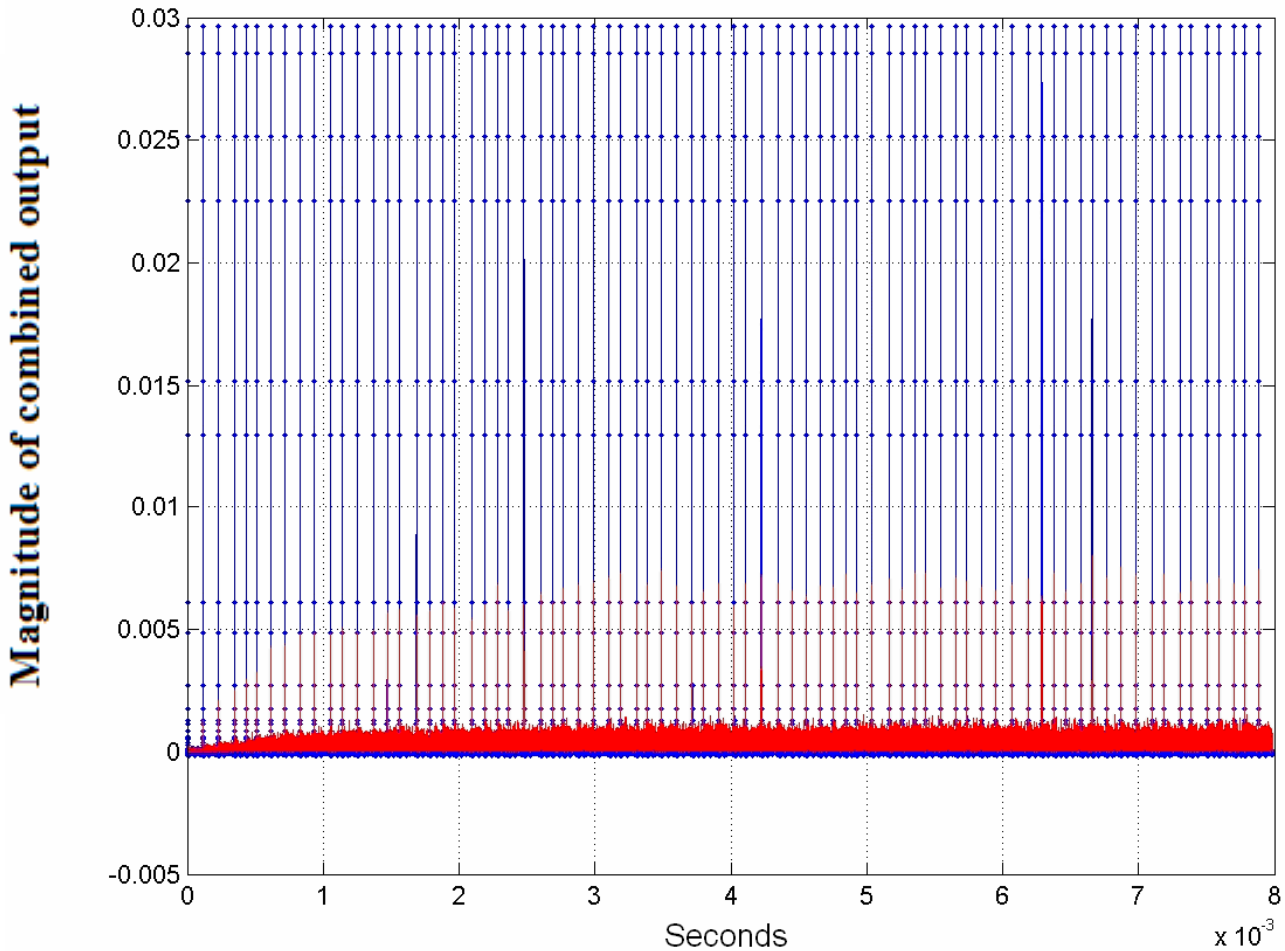

LMS Convergence

$$\mu = 1000 \qquad \mu_{\max} = 1.53 \cdot 10^3$$

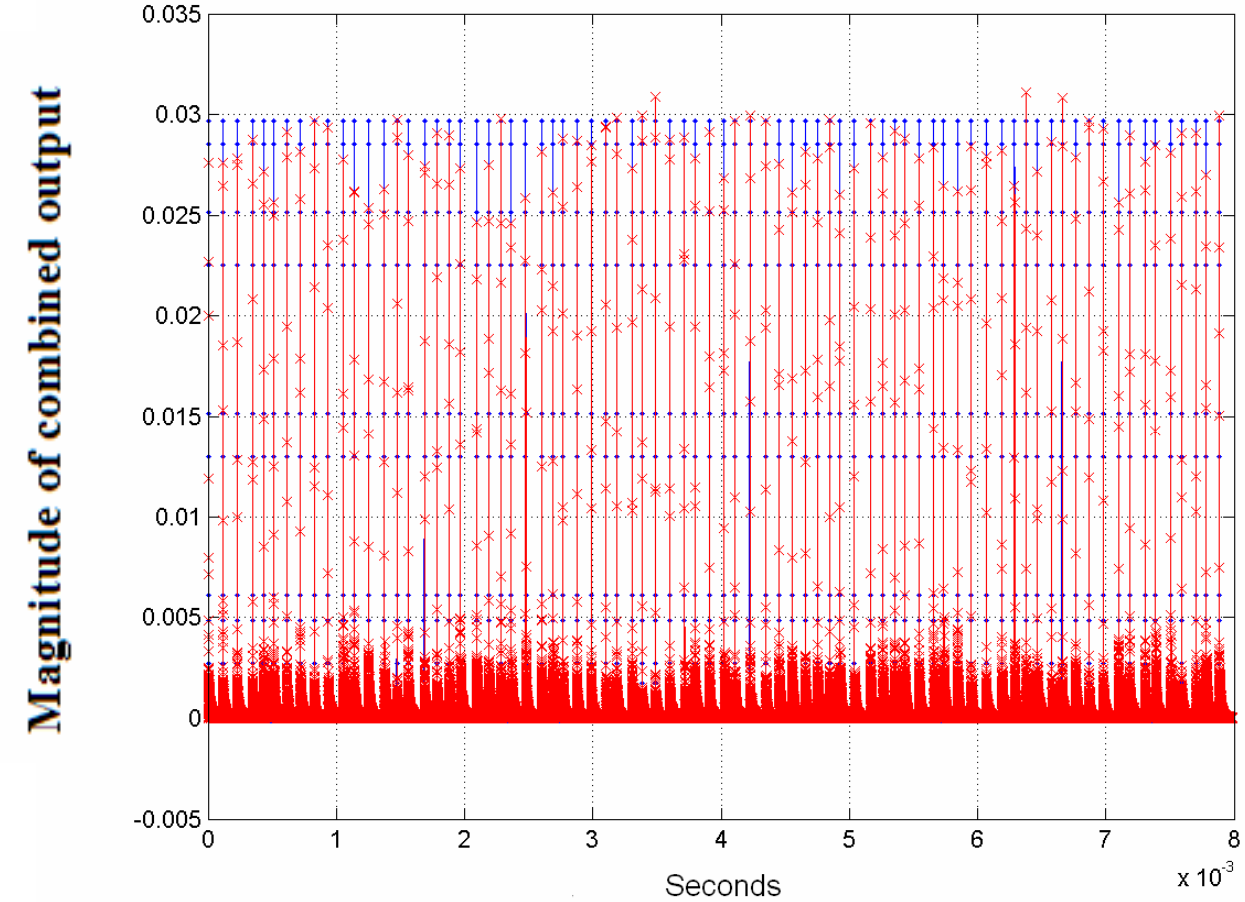

LMS Convergence

$$\mu = 10000 \qquad \mu_{\max} = 1.53 \cdot 10^3$$

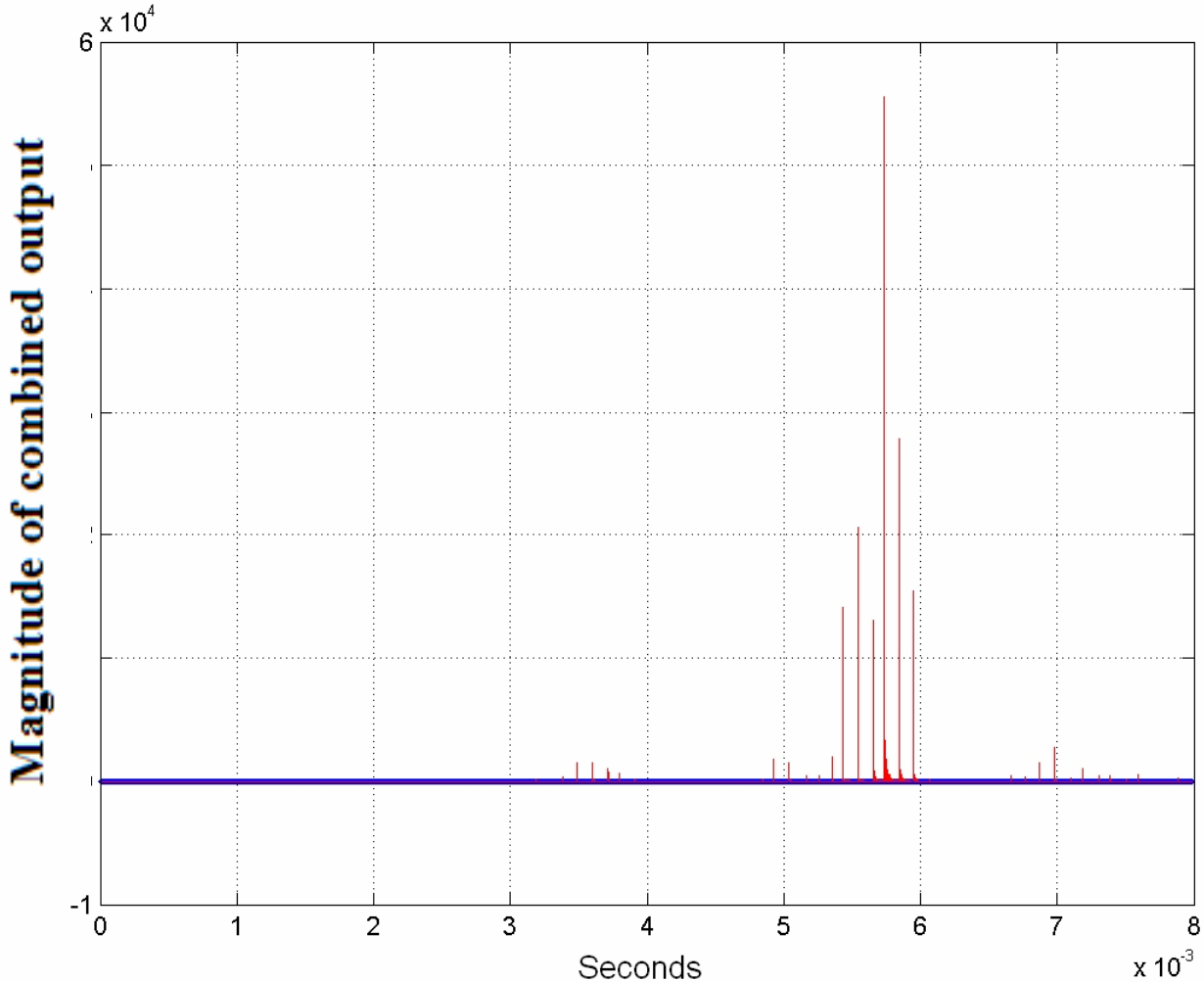

Phase of weights and channel

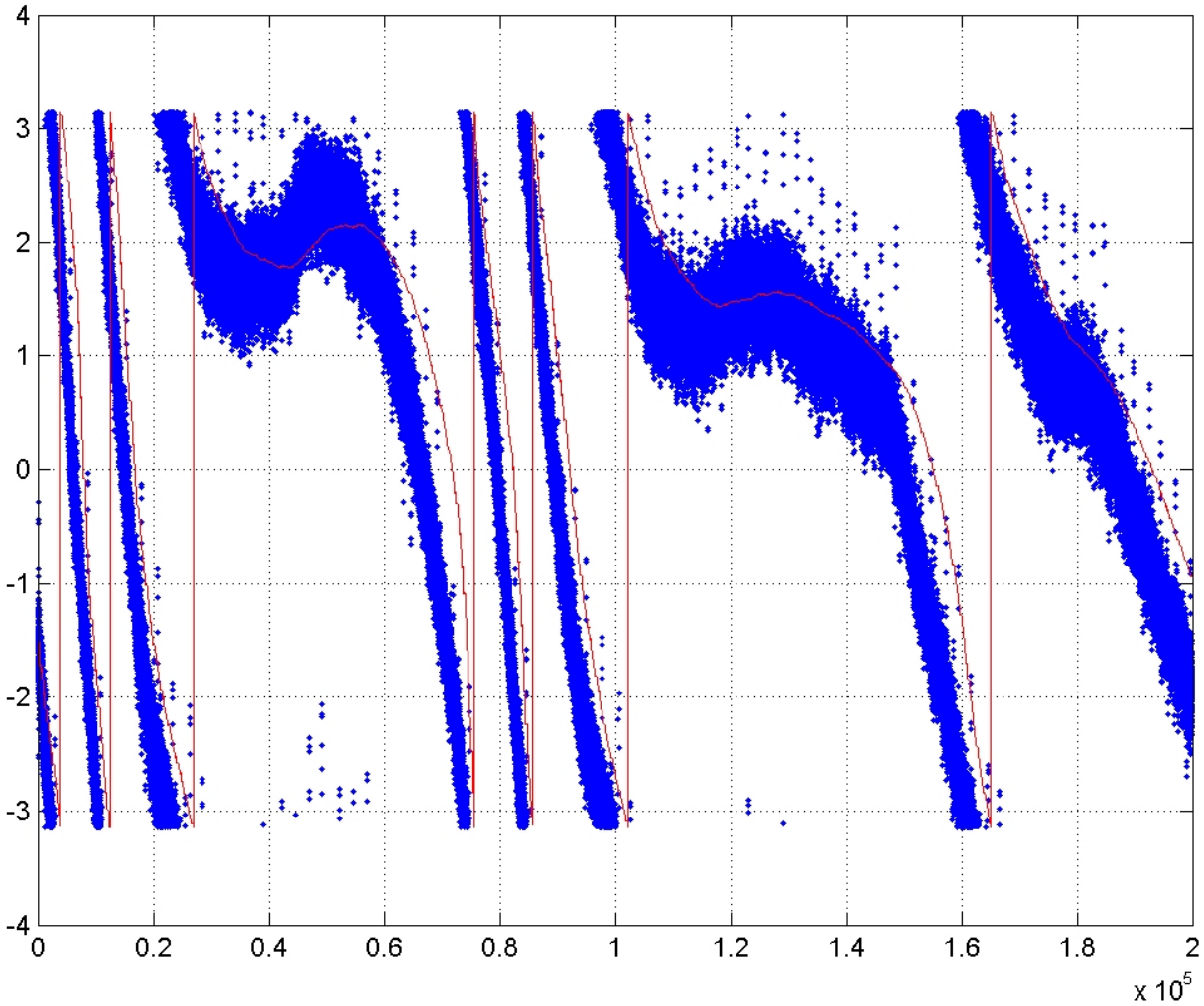

Convergence Test with Decision Feedback Errors

- Test objective
  - Determine the convergence behavior of LMS when decision feedback errors are made
  - Necessary since very large values of μ lead to fast convergence times and potentially serious issues in the face of decision feedback errors
- Test procedure
  - Intentionally introduce an error in the target sequence *d*(*k*)
  - Observe the effects on LMS convergence for $\mu \in \left\{10^{0.0}, 10^{0.1}, 10^{0.2}, \ldots, 10^{2.0}\right\}$
  - Exponential sweep chosen to allow rapid test of a range of μ over two orders of magnitude
- Test results
  - Require small values of μ
  - Converges for $\mu \leq 10^{0.8} \approx 6.3$

Successful Convergence with an Error

$$\mu = 10^{0.8} \approx 6.31$$

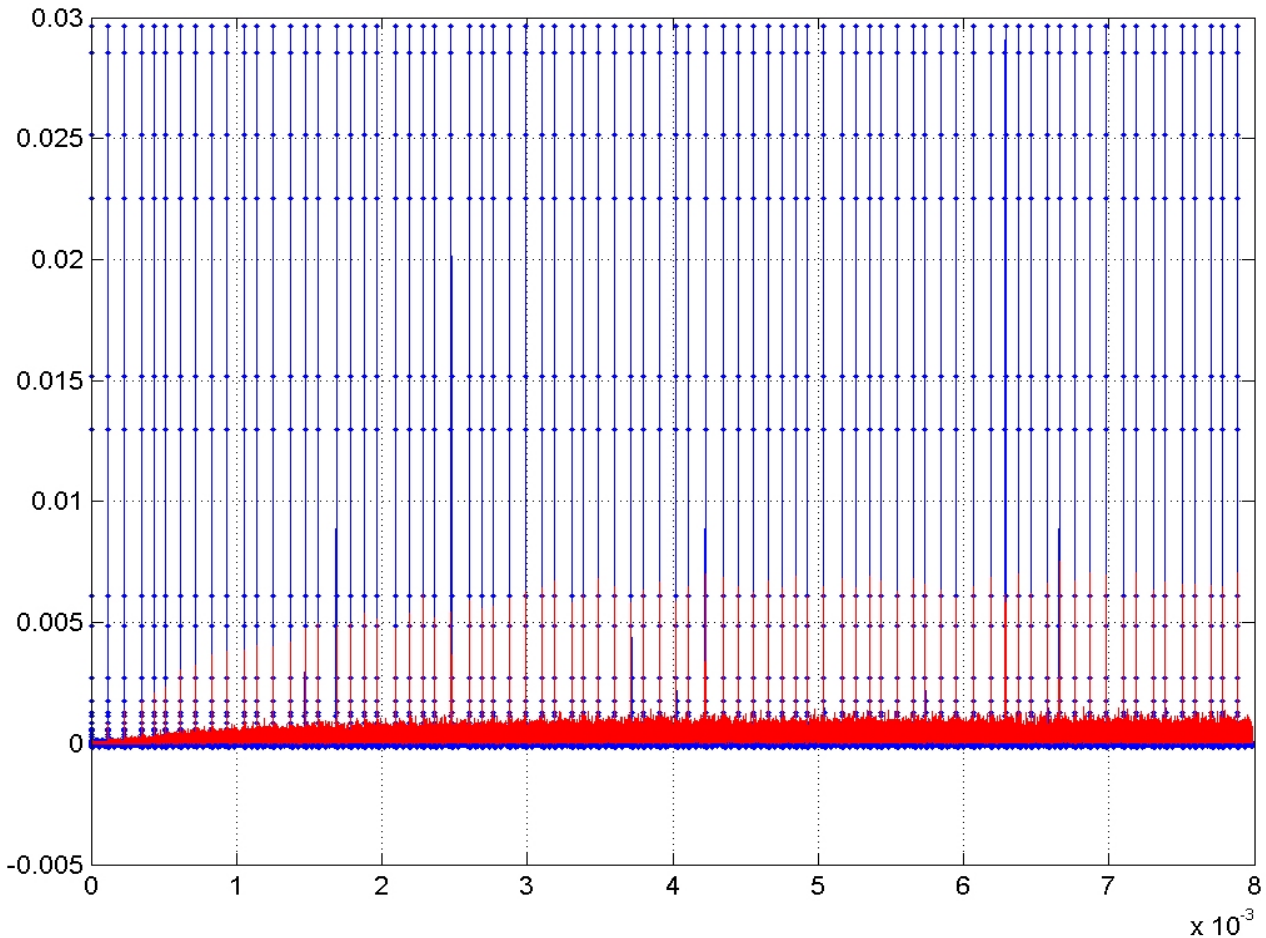

Divergence with an Error

$$\mu = 10^{0.9} \approx 7.94$$

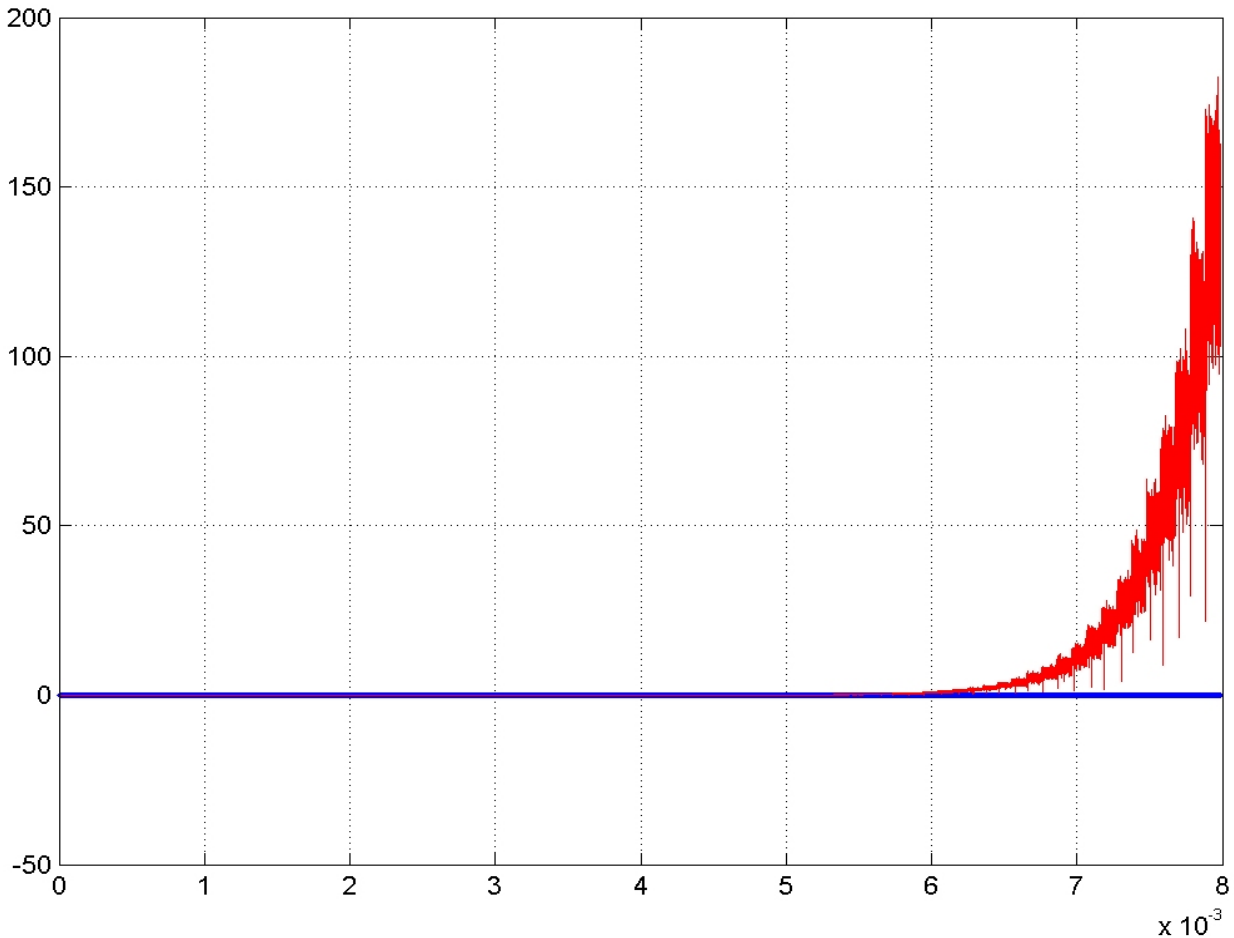

Single Detector 256 PPM BER vs. Ks

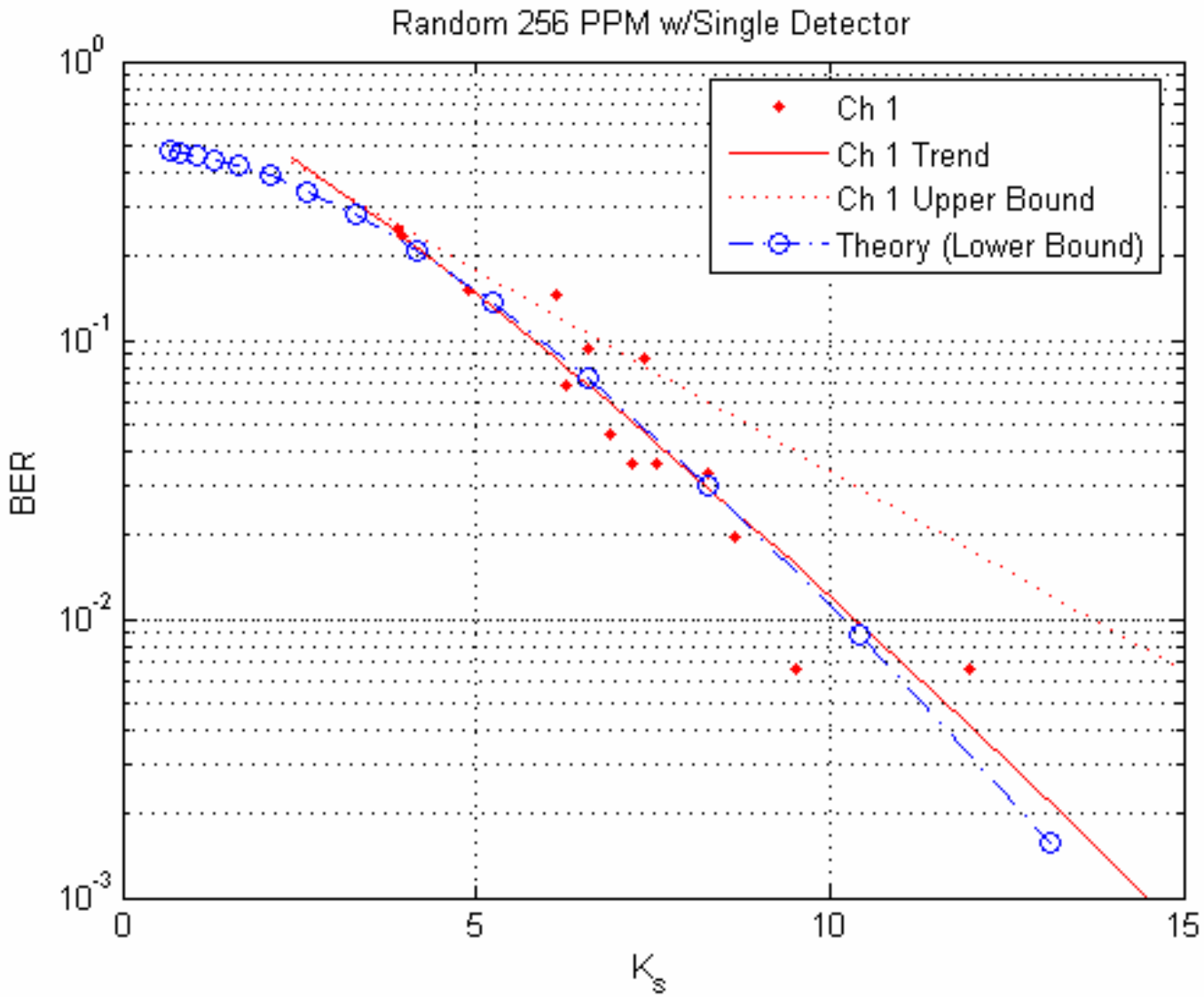

Single Detector 256 PPM
BER vs.(Photons per Bit)-PPB

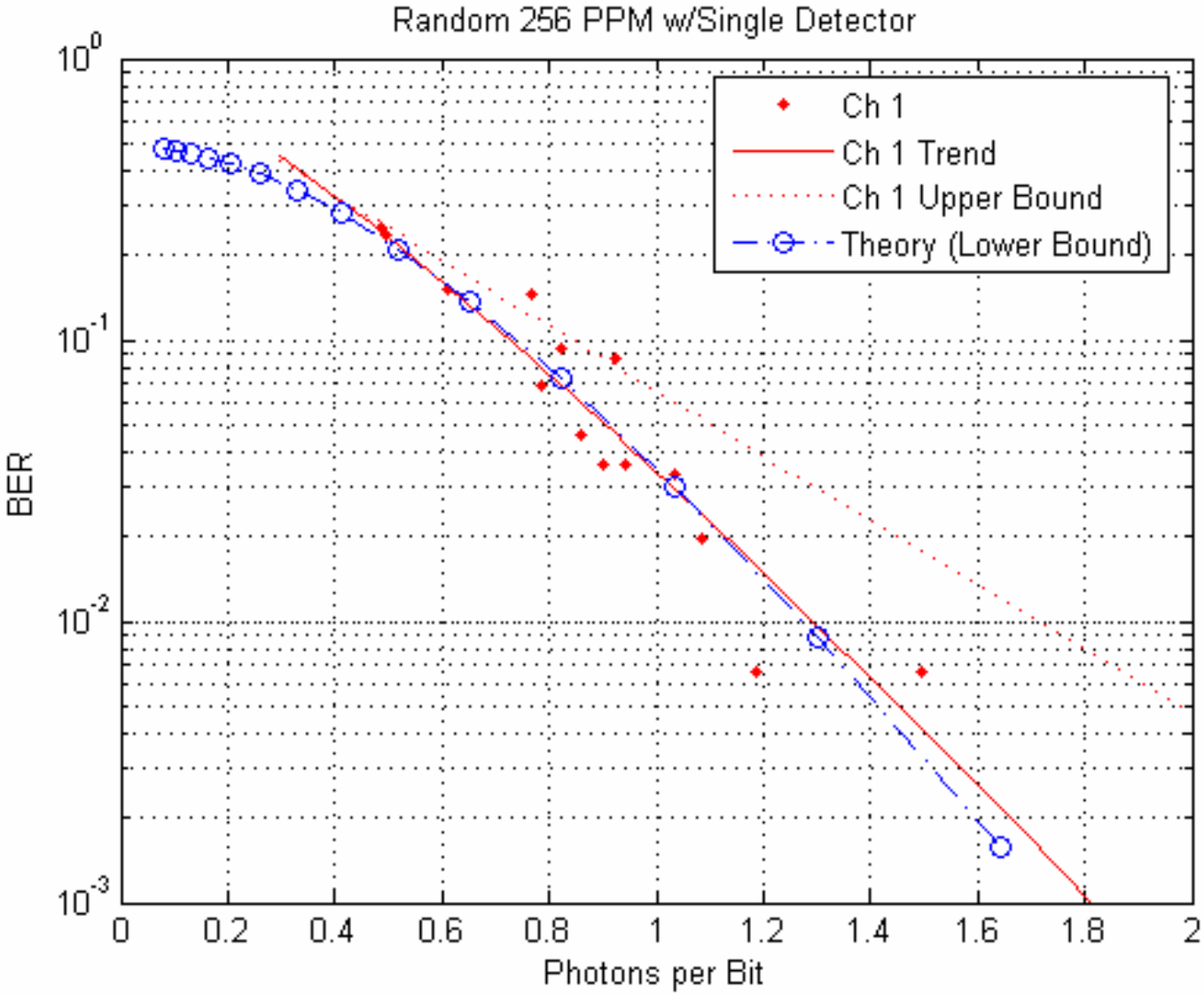

Single Detector 256 PPM
BER vs. Es/N0

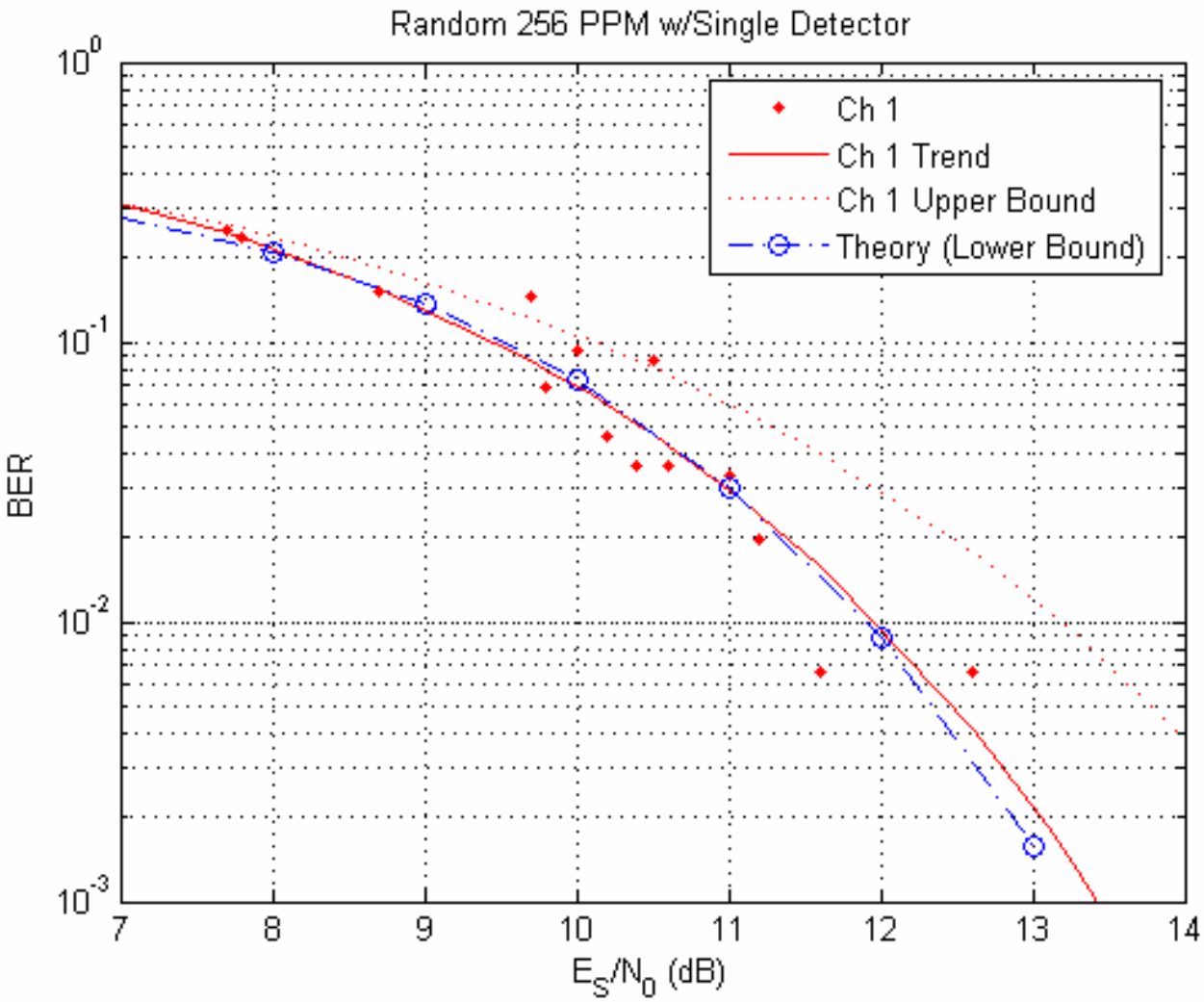

FPA 256 PPM- BER vs. Es/N0

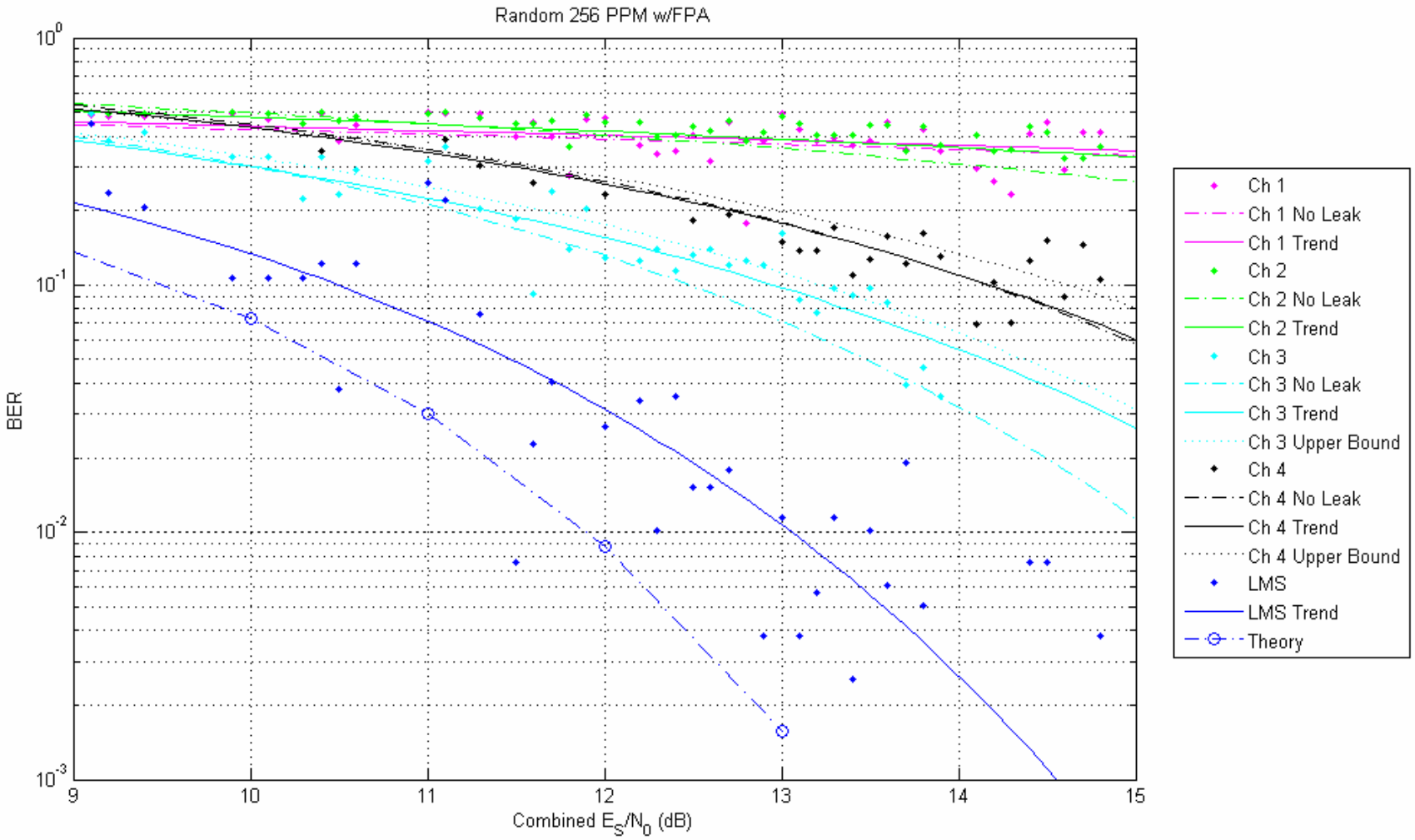

Hypothetical Shot Noise Limited FPA BER vs. Ks (256 PPM)

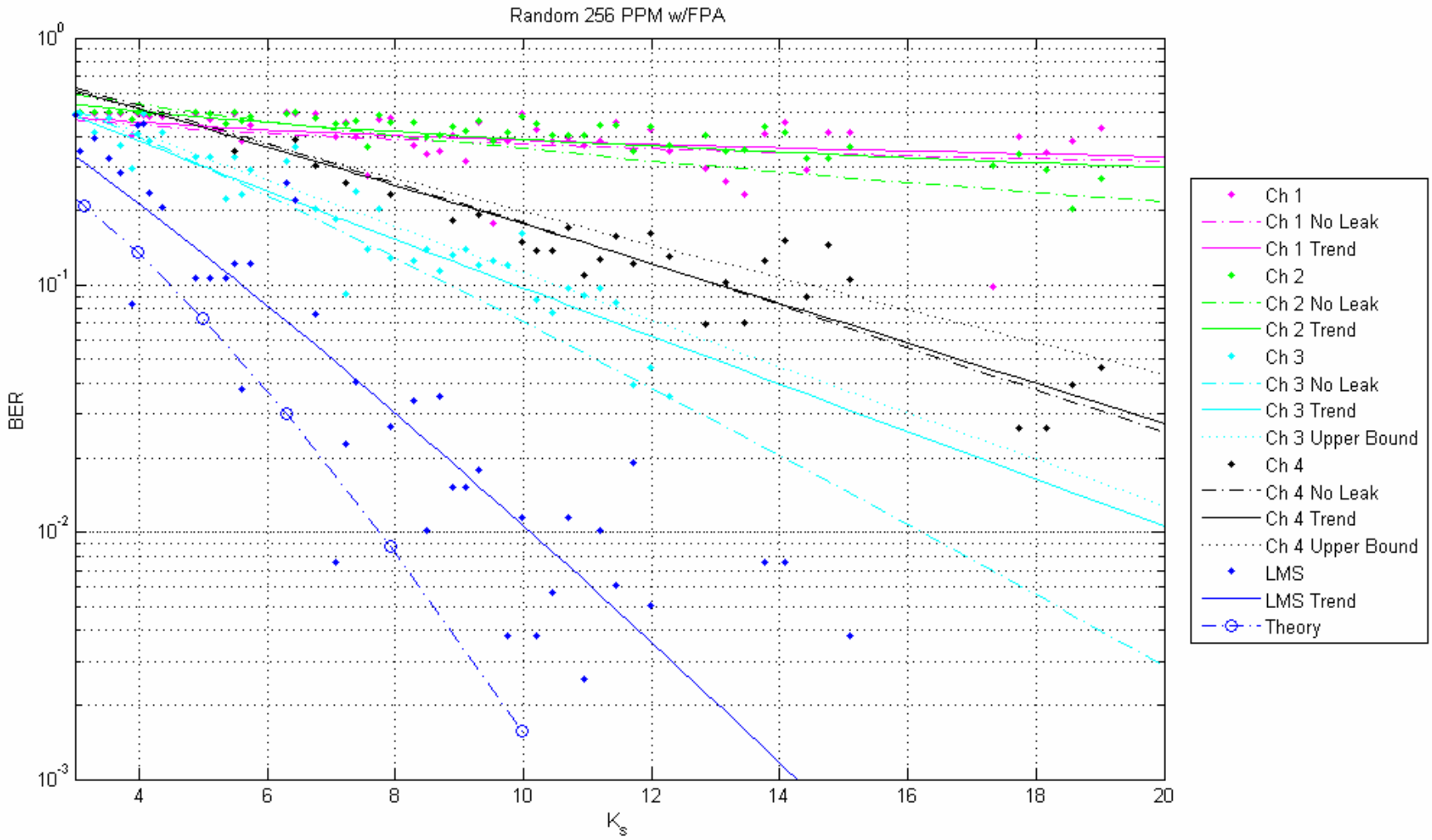

Hypothetical Shot Noise Limited FPA BER vs. Photons per Bit (256 PPM)

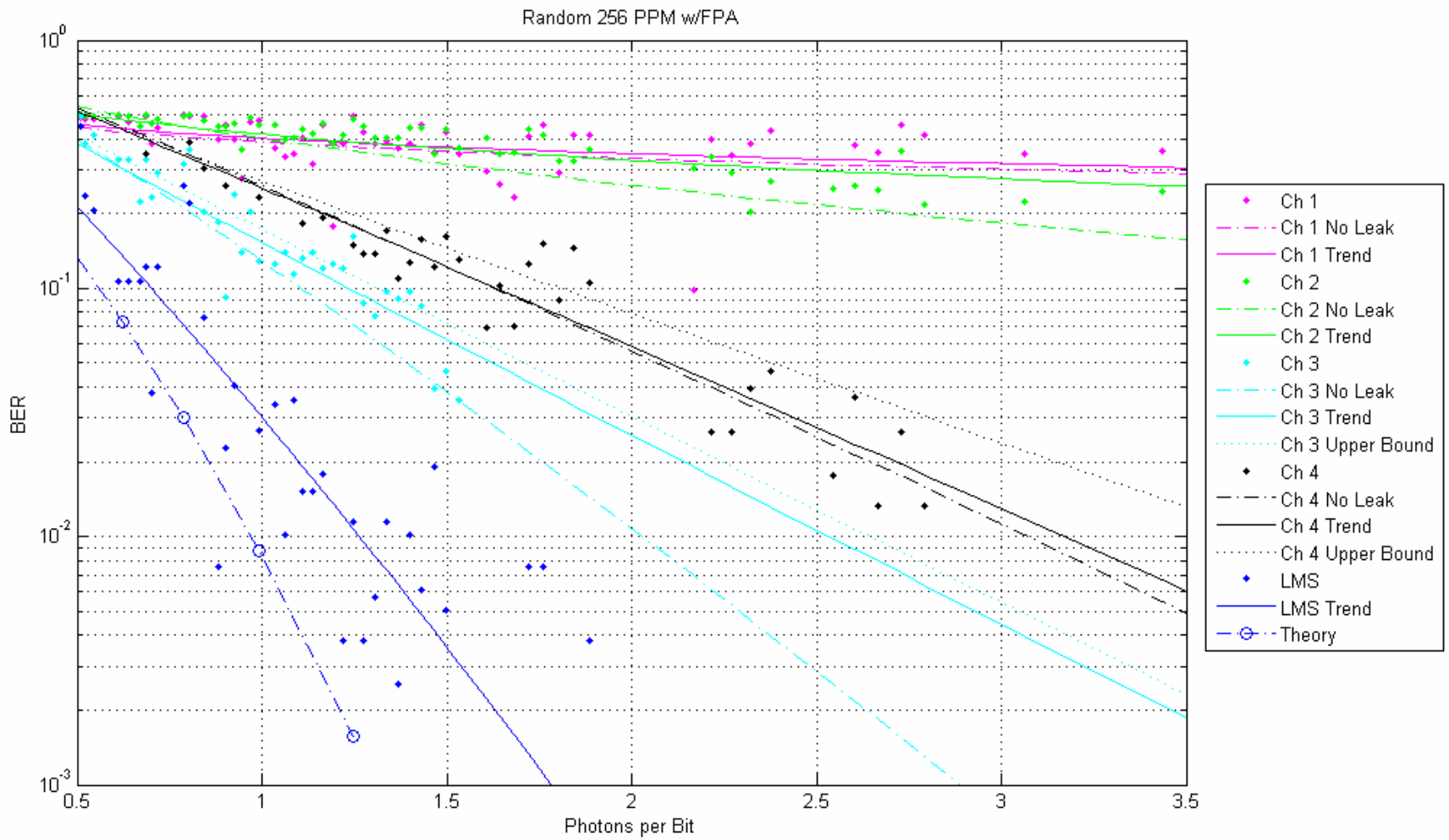

FPA with Good Detectors
BER vs. Ks (256 PPM)

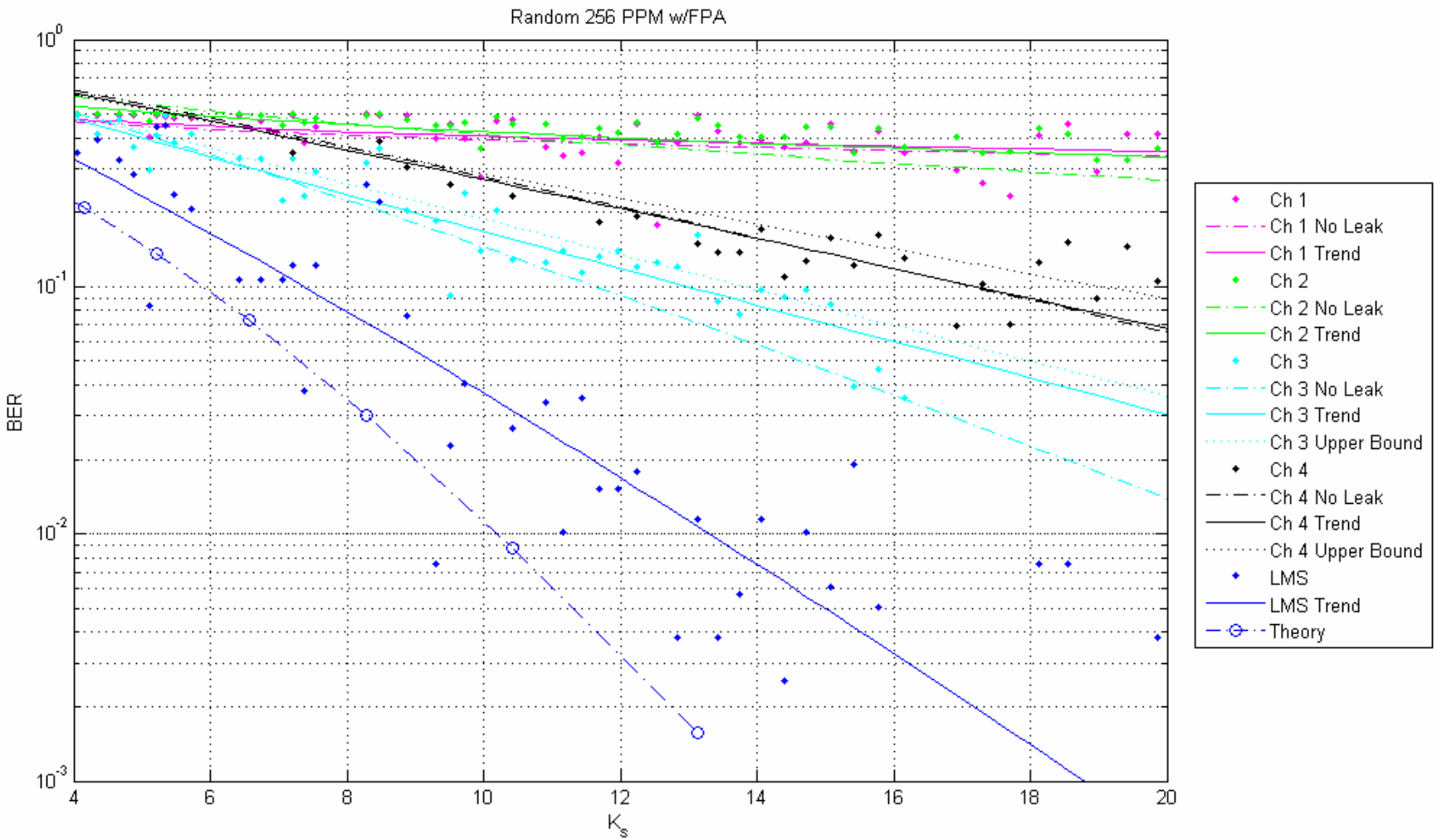

FPA with Good Detectors
BER vs. Photons per Bit (256 PPM)

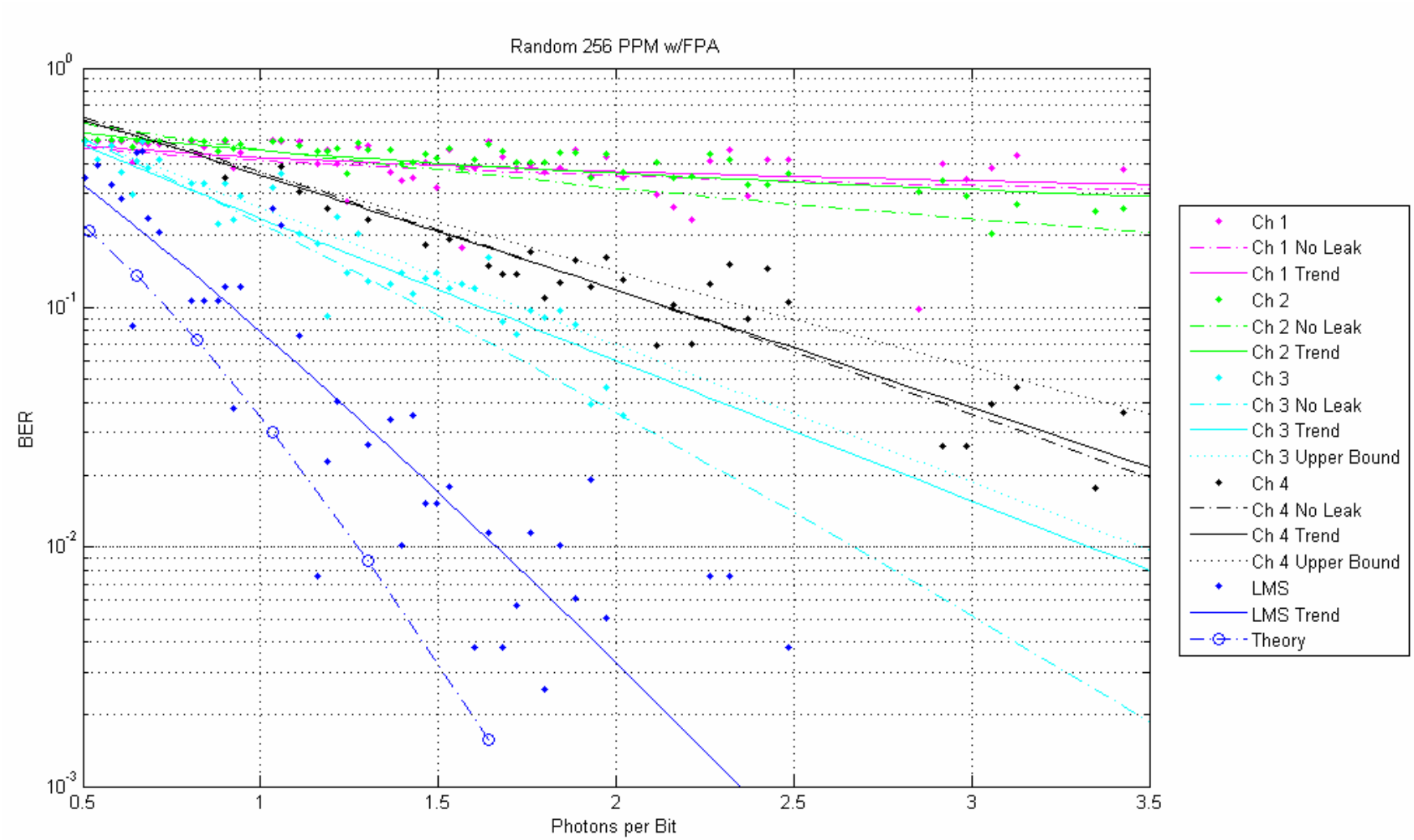

Actual FPA
BER vs Ks (256 PPM)

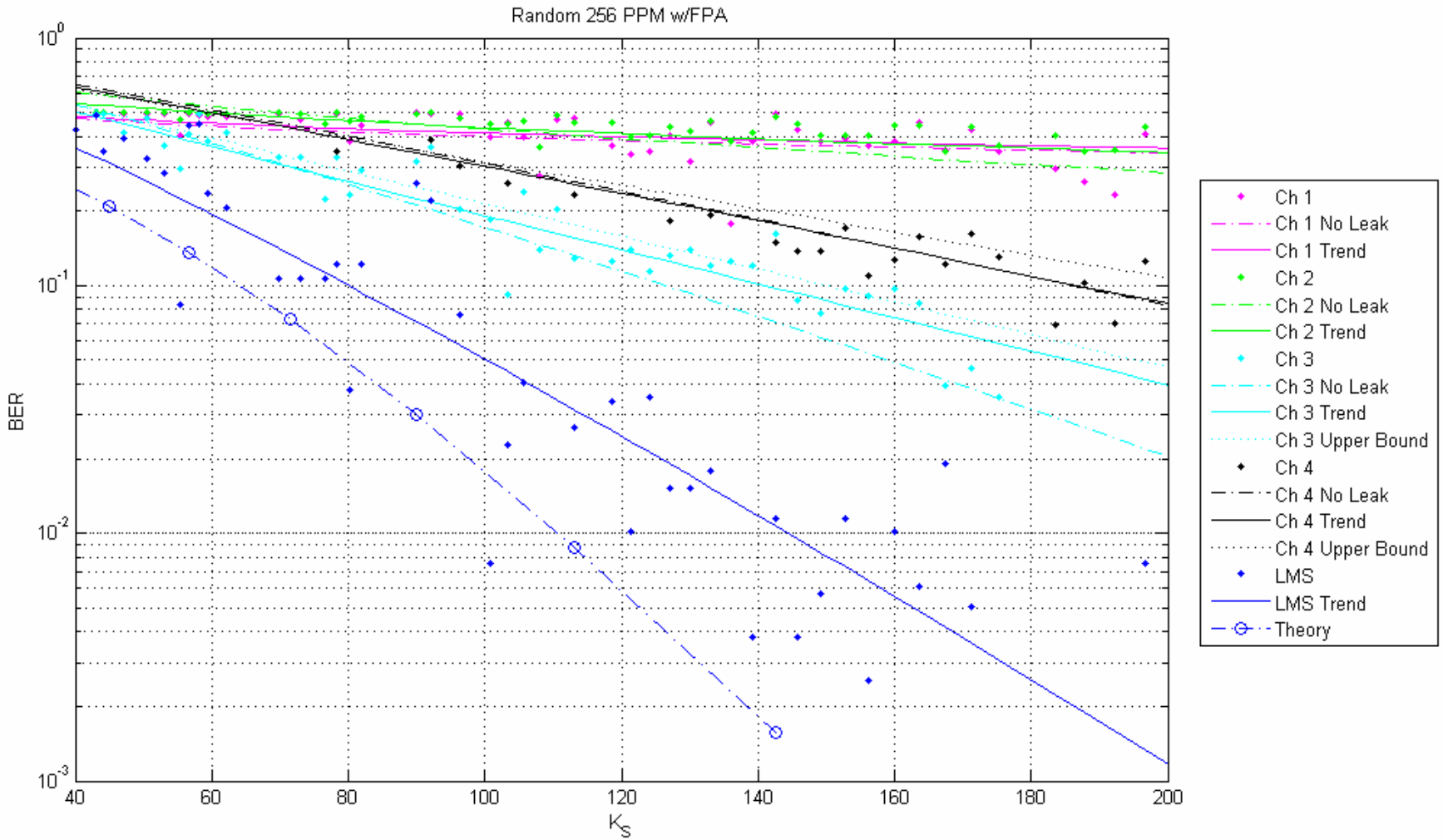

Actual FPA
BER vs. Photons per Bit (256 PPM)

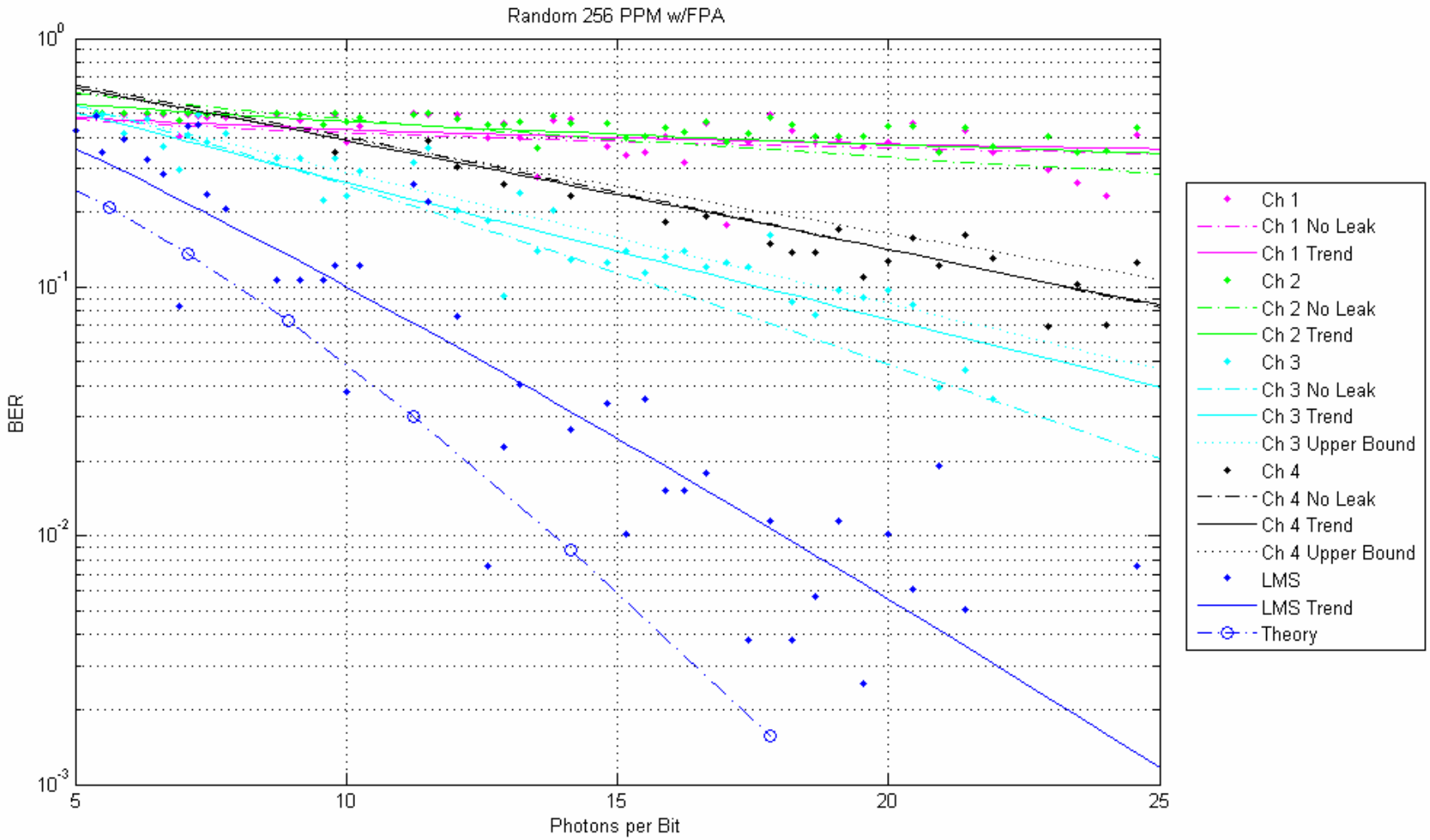

Conclusions and Future work

- In summary, the system designed presented herein has been shown, through both analysis and experiments, to have the potential to achieve BER performance 1dB away from the theoretical curve in the presence of weak signals and in the presence of distorted focal plane signal fields that result from phase distortions due to atmospheric turbulence

- The technology developed here can enable fundamental gains in the performance of deep space communication links by overcoming both weak signal limitations and signal degradation due to atmospheric phase distortions

Future directions

- Coherent combining algorithms for focal plane arrays. In a realistic space communications system utilizing PPM, the relative positions of the spacecraft and the ground receiver will change by many optical wavelengths between PPM pulses. Since no signal exists during the inter-pulse intervals, tracking of the spacecraft signal phase poses a special challenge.

- The use of coding would unleash the true potential of the focal plane array receiver. Uncoded bit error rates below are achievable using a shot-noise-limited receiver running at slightly less than one photon per bit. Corresponding coded bit error rates would be significantly lower, enabling very robust digital communications at low signal levels. The ability to communicate reliably at such weak signal levels would greatly extend the utility and usefulness of optical communications for deep space, especially in light of the severe demands generated by deep space link budgets.